Density-decomposed orbital-free density functional theory for covalently bonded molecules and materials

Junchao Xia and Emily A. Carter

Phys. Rev. B **86**, 235109 — Published 7 December 2012

DOI: 10.1103/PhysRevB.86.235109

Density-Decomposed Orbital-Free Density Functional Theory for Covalently Bonded Molecules and Materials

Junchao Xia[1] and Emily A. Carter[1, 2,*]

[1]Department of Mechanical and Aerospace Engineering, [2]Program in Applied and Computational Mathematics, and Andlinger Center for Energy and the Environment, Princeton University, Princeton, NJ 08544-5263

Abstract

We propose a density decomposition scheme using a Wang-Govind-Carter (WGC)-based kinetic energy density functional (KEDF) to accurately and efficiently simulate various covalently bonded molecules and materials within orbital free (OF) density functional theory (DFT). By using a local, density-dependent scale function, the total density is decomposed into a highly localized density within covalent bond regions and a flattened delocalized density, with the former described by semilocal KEDFs and the latter treated by the WGC KEDF. The new model predicts reasonable equilibrium volumes, bulk moduli, and phase ordering energies for various semiconductors compared to Kohn-Sham (KS) DFT benchmarks. The decomposition formalism greatly improves numerical stability and accuracy while retaining computational speed compared to simply applying the original WGC KEDF to covalent materials. The surface energy of Si(100) and various diatomic molecule properties can be stably calculated and also agree well with KSDFT benchmarks. This linear scaling, computationally efficient, density-partitioned/multi-KEDF scheme opens the door to large scale simulations of molecules, semiconductors, and insulators with OFDFT.

I. Introduction

In modern materials science and engineering modeling, first principles quantum mechanics methods are widely used because they can offer reliable results and predictions at the atomic scale, explaining many interesting phenomena that classical theories cannot. Among them, Kohn-Sham density functional theory (KSDFT)[1, 2] is the most popular one at present because of its excellent balance between accuracy and efficiency. However, orbital orthonormalization and k-point sampling in KSDFT typically make the computational cost scale cubically with respect to system size with a significant prefactor, effectively prohibiting extensive simulation of more than a few hundred atoms. Although many linear scaling KSDFT methods have been proposed,[3-10] most of them rely on orbital localization in insulators and hence are not applicable to metals. Furthermore, the relatively large prefactor of those linear scaling methods makes studying interesting large scale scientific problems still prohibitive with KSDFT, unless one has access to extraordinary computing resources.[11, 12]

On the other hand, an alternative DFT formalism, orbital-free density functional theory (OFDFT)[13] is a much more efficient first principles approach capable of treating much larger numbers of atoms. The Hohenberg-Kohn theorems[1] proved that the electron density uniquely determines the ground state of an electronic system, thereby providing the foundation for OFDFT, which uses the electron density as the basic variable. The number of degrees of freedom is thereby reduced from $3N$ electron coordinates to only three spatial coordinates, where N is the number of electrons in the system. OFDFT significantly decreases the computational cost, exhibiting quasi-linear scaling with system size with a small prefactor.[14, 15] A number of practical applications of OFDFT to predict mesoscale materials properties have been reported in recent years.[14-23] OFDFT provides an efficient and robust approach to study large samples with many

thousands of atoms, such as nanowire deformation,[18, 19] crack tip propagation,[20] and dislocation formation in metals.[16, 21]

However, a trade-off between accuracy and efficiency is inevitable. Instead of using orbitals to compute the electron kinetic energy, OFDFT uses approximate kinetic energy density functionals (KEDFs), which renders it less accurate than KSDFT in most cases. Only in some extreme limits like the uniform electron gas or a single orbital, are exact KEDF forms known: the local Thomas-Fermi (TF)[24-26] and the semilocal von Weizsäcker (vW)[27] KEDFs, respectively. The exact KEDF remains unknown. In recent decades, many forms of nonlocal KEDFs have been proposed, such as the Chacon-Alvarellos-Tarazona (CAT),[28-30] Wang-Teter (WT),[31] and Wang-Govind-Carter (WGC)[32, 33] functionals, etc.,[34-37] all based on Lindhard linear response theory.[38, 39] Some others involve higher-order response theories.[31, 40, 41] Generally, these KEDFs can model nearly-free-electron-like systems, such as main group metals and alloys, with accuracy comparable to KSDFT.[14-21, 33, 42-45] However, the narrow applicable area of current KEDF models inhibits OFDFT studies of many other interesting problems involving, e.g., semiconductors, transition metals, or molecules. In these latter cases, the electron density significantly deviates from the uniform electron gas scenario due to highly localized electrons. Consequently, the abovementioned nonlocal KEDFs become both physically and numerically unsound.[46] Only limited success was achieved when applying them to treat semiconductors or transition metals.[46-48]

Not until very recently have some successful OFDFT models been proposed for covalent materials and transition metals.[49-51] In 2010, the Huang-Carter (HC) KEDF[49] was proposed to account for the linear response properties of semiconductors, exhibiting much improved accuracy for bulk Si and III-V semiconductors and later for covalently-bonded molecules as

well.[52] The HC KEDF undoubtedly broadens OFDFT's range of applications. However, it still has several remaining drawbacks,[49] including insufficiently accurate properties of Si metallic phases, underestimated electron density in the bonding regions of Si and III-V semiconductors, unphysical shear moduli and self-interstitial formation energy. Furthermore, the optimal parameters in the HC KEDF change with the coordination number without a quantitative and systematic way to determine their values despite predicted qualitative trends.[49] Numerically, the HC functional employs interpolation to preserve the quasi-linear scaling,[50] which greatly increases the scaling prefactor, especially when density variations are large. For example, for a molecule or a solid surface with vacuum present in the periodic cell, an HC KEDF calculation can be hundreds of times slower than a WGC KEDF calculation. As a result, HC KEDF calculations on large systems containing large density variations become prohibitively time consuming. Therefore, an accurate *and* computationally efficient OFDFT model is still needed for covalently-bonded systems.

Among available nonlocal KEDFs, the WGC KEDF predicts exceptionally good results for light metals,[14-21, 33, 43, 44] which only involve small electron density variations. However, it describes covalently-bonded systems such as semiconductors or molecules far less accurately.[46, 52] In those systems, large density variations due to localized electrons challenge both the theoretical basis (the Lindhard response function of the perturbed free electron gas) and the numerical Taylor expansion.[46] However, an earlier re-parameterized WGC KEDF for various Si phases, though not entirely satisfactory for Si semiconductor phases,[46] features two positive aspects. First, it predicts rather reasonable equilibrium volumes, bulk moduli, and even total energies for Si metallic phases compared to KSDFT benchmarks, indicating the adequacy of the WGC KEDF for the level of density variation in those phases. Moreover, it generates reasonable

ground state densities even for Si semiconductor phases. Therefore, we expect that the incorrect energies for semiconductor phases mainly arise from the WGC KEDF approximation for regions featuring large density variations due to localized electrons in either tightly bound atomic orbitals or chemical bonds. The problem also appears for transition metals which feature highly localized d electrons around the nuclei. Recently, encouraging improvements towards extending OFDFT to transition metals have been made.[50, 51] These new models set up a volume around each atom that separates the localized (primarily d) electron density from the delocalized density and then treats each with different KEDF models. In a similar fashion, here we aim to decompose the electron density in covalently-bonded materials, treating the localized electron density in chemical bonding regions with local or semilocal KEDFs, while still describing the remaining delocalized electron density with the WGC KEDF. In this way, we hope to obtain an accurate but also efficiently evaluated model of covalent systems within OFDFT.

In the following, we first introduce in Section II the WGC-KEDF-based density decomposition formalism, in which we use the total density as a metric to identify localized electrons, and then further decompose the electron density. Different KEDF models are then used to separately treat localized and delocalized electron densities. The numerical details are described thereafter in Section III. Section IV presents test of the model for different covalently bonded systems including bulk Si and III-V semiconductors, as well as diatomic molecules. The conclusions are given in Section V.

II. Formalism

According to the Hohenberg-Kohn theorems,[1] the electronic total energy is a functional of the total electron density, ρ_{total}:

$$E[\rho_{\text{total}}] = T_{\text{s}}[\rho_{\text{total}}] + J[\rho_{\text{total}}] + E_{\text{xc}}[\rho_{\text{total}}] + \int V_{\text{ext}}(\mathbf{r})\rho_{\text{total}}(\mathbf{r})d\mathbf{r} \text{ . (1)}$$

Here T_{s} is the non-interacting electron kinetic energy, J is the Hartree electron-electron repulsion energy, and E_{xc} is the electron exchange-correlation energy. V_{ext} is the external potential, such as electron-ion pseudopotentials in the present calculations.

As discussed above, electrons localized in chemical bonds lead to large density variations in covalently bonded systems. Table I shows the ratio of the maximum density to the average density in different physical systems, which to some extent reflects the respective level of density variation. We observe that covalent materials such as cubic diamond (CD) and hexagonal diamond (HD) Si feature significantly higher ratios than metallic Si phases, Al, or Mg. To apply the WGC KEDF to these covalently-bonded materials, we introduce an electron density decomposition formalism, where we separate localized and delocalized electron densities, describing the localized part with semilocal KEDFs and treating only the delocalized component with the WGC functional. We refer to this method as the WGCD model in what follows.

In each calculation, we define a scale function $F(\mathbf{r})$ over all space. The delocalized electron density ρ_{del} is then computed as:

$$\rho_{\text{del}}(\mathbf{r}) = \rho_{\text{total}}(\mathbf{r}) \times F(\mathbf{r}) \text{ . (2)}$$

Accordingly,

$$\rho_{\text{loc}}(\mathbf{r}) = \rho_{\text{total}}(\mathbf{r}) - \rho_{\text{del}}(\mathbf{r}) \text{ , (3)}$$

where ρ_{loc} is the localized electron density. After decomposing the density, the kinetic energy is calculated as:

$$T_{\text{s}}[\rho_{\text{total}}] = (T_{\text{s}}[\rho_{\text{total}}] - T_{\text{s}}[\rho_{\text{del}}]) + T_{\text{s}}[\rho_{\text{del}}] \text{, (4)}$$

similar to previous work for transition metals.[50] We can re-write the two terms in parentheses as:

$$T_s[\rho_{total}] - T_s[\rho_{del}] = T_s[\rho_{loc}] + (T_s[\rho_{total}] - T_s[\rho_{del}] - T_s[\rho_{loc}]) . \quad (5)$$

In this way, we can identify these two terms as the localized electron kinetic energy (first term on the right hand side of Eq. 5) and the interaction kinetic energy between localized and delocalized electrons (second term on the right hand side of Eq. 5). One may recognize the latter interaction term from embedding theories or as the non-additive KEDF (T_{nad}).[53] A number of T_{nad} models exist in the literature,[53-56] which generally utilize complicated forms of enhancement factors with the reduced density gradient. In this work, we mainly aim to test the physics of the decomposition formalism, so we simply employ the semilocal $aT_{TF} + bT_{vW}$ KEDF model for the interaction kinetic energy as well as for the localized kinetic energy terms, which has been justified in previous literature.[50, 53, 56-59] For the last term on the right hand side of Equation (4), the delocalized electron kinetic energy, we utilize the WGC KEDF, since it should possess the correct physics for those electrons. The total kinetic energy is now approximated as

$$T_s[\rho_{total}] = (T_s^{semilocal}[\rho_{total}] - T_s^{semilocal}[\rho_{del}]) + T_s^{WGC}[\rho_{del}] . \quad (6)$$

The corresponding kinetic energy potential is also easily derived:

$$\frac{\delta T_s[\rho_{total}]}{\delta \rho_{total}} = \left[\frac{\delta T^{semilocal}[\rho_{total}]}{\delta \rho_{total}} - \frac{\delta T^{semilocal}[\rho_{del}]}{\delta \rho_{del}} \cdot F(\mathbf{r}) \right] + \frac{\delta T^{WGC}[\rho_{del}]}{\delta \rho_{del}} \cdot F(\mathbf{r}) . \quad (7)$$

It is evident that the scale function $F(\mathbf{r})$ largely determines the quality of the resulting KEDF. Two limits of $F(\mathbf{r})$ are 1 and 0. $F(\mathbf{r}) \equiv 1$ makes the formalism recover the original WGC KEDF as $\rho_{loc} = 0$; while for $F(\mathbf{r}) \equiv 0$, the KEDF becomes the simple semilocal model as

$\rho_{\text{del}} = 0$. In transition metals, a sphere around the nuclei can be easily defined to treat localized d electrons separately, as done in previous models,[50, 51] where the scale function *F* depends only on the spatial coordinates explicitly. However, the location of localized electrons in covalently-bonded systems is different. For example, CD Si has localized electrons between each pair of atoms. In a general material or molecule, one cannot identify regions of localized density by an obvious atom-centered object such as a simple sphere. In order to locate localized electrons and further decompose the total density, spatial coordinates alone are insufficient. It is straightforward to make use of other information from the electron density, the energy density or the energy potential, like in the electron localization function (ELF)[60, 61] in KSDFT. Although the ELF is an ideal indicator of electron localization and a metric to determine $F(\mathbf{r})$, unfortunately OFDFT lacks the orbital information or KSDFT kinetic energy density $\tau(\mathbf{r})$, required to evaluate the ELF. Therefore, we need to find another metric to determine $F(\mathbf{r})$.

In fact, the total electron density itself could reasonably reveal electron localization, since the electron density should be large where electrons are localized. As Figure 1 demonstrates, ρ_{total} shares a similar shape to the ELF. Therefore, we employ ρ_{total} as an indicator to calculate $F(\mathbf{r})$. In practice, we choose the dimensionless quantity $\rho_{\text{total}} / \rho_0^{\text{del}}$ as the argument, where ρ_0^{del} is the average of the delocalized density, explicitly written as

$$F(\mathbf{r}) = f(\rho_{\text{total}}(\mathbf{r}) / \rho_0^{\text{del}}), \quad (8)$$

where $f(\rho_{\text{total}}(\mathbf{r}) / \rho_0^{\text{del}})$ is bounded between 0 and 1.

In this work, we choose a numerical form of $f(\rho_{\text{total}}(\mathbf{r}) / \rho_0^{\text{del}})$ (see Figure 2) to physically separate localized and delocalized electron densities. It features several desirable properties: (i) if

$\rho_{\text{total}}(\mathbf{r})/\rho_0^{\text{del}} \le 1$, $f(\rho_{\text{total}}(\mathbf{r})/\rho_0^{\text{del}}) \approx 1$, while it decreases as $\rho_{\text{total}}(\mathbf{r})/\rho_0^{\text{del}}$ increases and $f(\infty) \to 0$. This guarantees that ρ_{loc} appears only in chemical bonding or atomic core regions (where $\rho_{\text{total}}(\mathbf{r})/\rho_0^{\text{del}}$ is large), and $\rho_{\text{del}} \approx \rho_{\text{total}}$ in interstitial volumes (where $\rho_{\text{total}}(\mathbf{r})/\rho_0^{\text{del}}$ around or smaller than 1). (ii) It usually generates a flattened, delocalized density ρ_{del} with $\rho_{\text{max}}^{\text{del}}/\rho_0^{\text{del}} \le 1.5$, typical for metallic phases that the WGC KEDF is able to describe well (Table 1), where $\rho_{\text{max}}^{\text{del}} = \max(\rho_{\text{del}})$. For CD Si, we obtain a much flatter ρ_{del} than the original ρ_{total}, with significantly smaller density variations (see Figure 3). (iii) $f(\rho_{\text{total}}(\mathbf{r})/\rho_0^{\text{del}})$ possesses appealing self-consistency properties in limiting cases. In the limit of nearly-free-electron-like systems $(\rho_{\text{del}} \approx \rho_{\text{total}})$, $F(\mathbf{r}) = f(\rho_{\text{total}}(\mathbf{r})/\rho_0^{\text{del}}) \approx 1$ thus leading to $\rho_{\text{del}} \approx \rho_{\text{total}}$ self-consistently. On the other hand, in the limit of a completely localized density ($\rho_{\text{del}} \approx 0$), $\rho_{\text{total}}(\mathbf{r})/\rho_0^{\text{del}} \to \infty$ and $F(\mathbf{r}) = f(\rho_{\text{total}}(\mathbf{r})/\rho_0^{\text{del}}) \approx 0$, thus leading to $\rho_{\text{del}} \approx 0$ self-consistently.

To increase the flexibility of the scale function, we introduce a shift parameter *m*,

$$F(\mathbf{r}) = f(\rho_{\text{total}}(\mathbf{r})/\rho_0^{\text{del}} - m) = f(\zeta), \; f(\zeta < 0) \equiv 1, \quad (9)$$

where we define the argument of the *f* function as ζ. Large *m* leads to a small ζ and thus large $F(\mathbf{r})$ (up to the upper bound of 1). Physically, this corresponds to less scaling and decomposition, which should be expected when simulating metallic phases, as will be shown in the following sections.

Finally, since the presence of ρ_0^{del} in the scale function makes it difficult to fully evaluate the functional derivative of $F(\mathbf{r}) = f(\zeta)$ with respect to ρ_{total}, we assume $F(\mathbf{r})$ depends only on spatial coordinates and employ Equation (7) to evaluate the kinetic energy potential. We

therefore have to introduce an extra loop to guarantee full self-consistency of $F(\mathbf{r})$ so that the assumption becomes true at convergence. Specifically, we use a pure WGC ground state density as a starting guess to obtain the initial $F(\mathbf{r})$, as the WGC KEDF yields reasonable densities compared to KSDFT (see Figure 1). We then perform a density decomposition calculation using this predetermined, fixed $F(\mathbf{r})$. Once we obtain converged, new, total and delocalized densities from the decomposition calculation, we re-calculate $F(\mathbf{r})$ to start a new iteration. We loop this procedure until $F(\mathbf{r})$ becomes self-consistent (see flow chart, Figure 4). We find that different choices for the delocalized KEDF model in the first iteration do not influence the final results. Consequently, other KEDFs, such as the WT KEDF, can also be used in the first iteration. The WT KEDF also predicts a reasonable density distribution (see Figure 1) and always converges, which is not always the case for the pure WGC KEDF used on the total density. After the first iteration, we switch to the WGC KEDF to describe the delocalized electron density. Since neither the WGC KEDF (for delocalized electron densities) nor the semilocal model (for localized electron densities) diverges, this new formalism is always stable.

III. Numerical details

We perform OFDFT calculations with our PROFESS 2.0 code[14, 62] and KSDFT computations with the ABINIT code.[63] The Perdew-Zunger (PZ) local density approximation (LDA) exchange-correlation (XC) functional is employed in all calculations.[64, 65] We aim here to simply compare the accuracy of our new KEDF scheme against KSDFT kinetic energy benchmarks; hence we do not bother to perform calculations with a more accurate, generalized gradient approximation XC functional, although it is available in our code. In both OFDFT and KSDFT calculations, bulk-derived local pseudopotentials (BLPSs)[66] reported in previous literature are used.[49, 67]

We study bulk properties of CD, HD, complex body-centered-cubic (cbcc), β-tin, body-centered-tetragonal (bct5), simple cubic (sc), hexagonal-close-packed (hcp), body-centered-cubic (bcc) and face-centered-cubic (fcc) phases of Si, as well as cubic zinc blende (ZB) and hexagonal wurtzite (WZ) structures of III-V semiconductors including AlP, AlAs, AlSb, GaP, GaAs, GaSb, InP, InAs, and InSb. The structural details were given in previous work.[49, 67]

In the KSDFT calculations, a kinetic energy cutoff for the plane wave basis of 900 eV is used to converge the total energy to within 1 meV/atom. For various Si and III-V semiconductor calculations, k-point meshes are generated with the Monkhorst-Pack method.[68] Table II lists the detailed k-point meshes and the Fermi-Dirac smearing widths. These k-point meshes converge the CD Si elastic constants to within 0.2 GPa, based on the difference between using the $12\times12\times12$ mesh in Table II and a much denser $30\times30\times30$ mesh. The k-point meshes are decreased when calculating vacancy and self-interstitial formation and surface energies to keep the k-point spacing consistent with what is used in bulk CD Si calculations. The details for diatomic molecule calculations are the same as given in our previous work.[52] In all OFDFT calculations, a 6000 eV plane wave kinetic energy cutoff is used to achieve convergence of 1 meV/atom. The scale function is considered self-consistent if $\max(\left|F_{[i]}(\mathbf{r})-F_{[i-1]}(\mathbf{r})\right|)<\xi$ (the subscript in square brackets represents the iteration step). We set ξ equal to 10^{-4} in all calculations, which guarantees convergence to within 10^{-2} meV/atom.

A number of parameters must be selected for the KEDFs in OFDFT calculations. We use the universally-derived density exponents $\alpha=(5-\sqrt{5})/6$ and $\beta=5/3-\alpha$ in the WGC KEDF.[33] γ is set equal to 3.6 for all calculations, as optimized for the CD Si phase in previous work.[46] In the WGCD calculation of the delocalized density, the WGC kernel is re-evaluated

each iteration according to that iteration's ρ_0^{del}. In all bulk crystal calculations, ρ_0^{del} is simply computed as the average of ρ_{del}, which is also used as the Taylor expansion center ρ_*. In surface and molecule calculations, this definition fails due to the large region of vacuum in the supercell. In such calculations, ρ_0^{del} is calculated as the average of ρ_{del} only in an effective region where ρ_{del} is larger than a critical value ρ_{c}. In our Si(100) surface calculations, ρ_{c} is set equal to 0.00684 a.u., which is the minimum density in bulk CD Si at its equilibrium volume. For diatomic molecule calculations, no obvious choice of ρ_{c} exists. The value is adjusted for different diatomics. We set $\rho_* = \frac{2}{3}\rho_{\mathrm{max}}^{\mathrm{del}}$, a typical relation in bulk calculations, to produce good numerical stability. Three other parameters must be chosen in the decomposition formalism: the coefficients *a* for the TF KEDF and *b* for the vW KEDF, as well as the shift parameter *m* in the scale function. They are first slightly tuned when calculating different properties but we also test a universal, average set of parameters in what follows. In the HC KEDF calculations (performed for comparison) of CD Si elastic constants and surface energies, we used parameters optimized previously for CD Si, λ=0.01 and β=0.65.[49] Finally, when we use the original WGC KEDF to calculate CD Si elastic constants, we select the default α and β values given above and employ $\rho_* = \rho_0$ and γ=3.6.

We calculated equilibrium volumes, bulk moduli, and phase energy differences for all Si and III-V semiconductor phases. Equilibrium structures are fully relaxed in KSDFT calculations using the default force and stress thresholds in the ABINIT code. Since the stress expression for the WGCD KEDF has not been implemented yet within PROFESS, we manually optimize the OFDFT geometries by scanning the degrees of freedom (one or two) in each structure. After

obtaining the relaxed equilibrium structure, we expand and compress the equilibrium volume by up to 2% to compute eight energy-volume points and then fit to Murnaghan's equation of state[69] to compute the bulk modulus. The phase energy differences are just the total energy differences between phases at their equilibrium structures. We also calculate the phase transition pressure (P_{trans}) using the common tangent rule,

$$\left.\frac{dE}{dV}\right|_{\text{phase 1}} = \left.\frac{dE}{dV}\right|_{\text{phase 2}} = -P_{\text{trans}} \,. \quad (10)$$

To calculate other elastic constants for CD Si, we apply a strain tensor, ε, to the equilibrium structure:[70]

$$\begin{pmatrix} a'_1 \\ a'_2 \\ a'_3 \end{pmatrix} = \begin{pmatrix} a_1 \\ a_2 \\ a_3 \end{pmatrix} \cdot (\mathbf{1} + \varepsilon) \,, \quad (11)$$

where a_{i} are primitive vectors and

$$\varepsilon = \begin{pmatrix} e_{xx} & \frac{e_{xy}}{2} & \frac{e_{zx}}{2} \\ \frac{e_{xy}}{2} & e_{yy} & \frac{e_{yz}}{2} \\ \frac{e_{zx}}{2} & \frac{e_{yz}}{2} & e_{zz} \end{pmatrix} , \quad (12)$$

where e_{ij} are strain components defined in Cartesian coordinates. For the tri-axial shear modulus C_{44}, we apply the tri-axial shear strain e=(e_{xx},e_{yy},e_{zz},e_{yz},e_{xz},e_{xy}) =(0,0,0,δ,δ,δ) to the equilibrium structure with δ up to 2%. Then C_{44} is calculated by fitting to the form:

$$\frac{\Delta E}{V} = \frac{3}{2} C_{44} \delta^2 \,. \quad (13)$$

Similarly, for the orthorhombic shear modulus C', we apply the volume-conserving orthorhombic strain $e=(\delta,\delta,(1+\delta)^{-2}-1,0,0,0)$ and calculate by fitting the equation:

$$\frac{\Delta E}{V} = 6C'\delta^2 . \quad (14)$$

C_{11} and C_{12} are then computed according to the relations:

$$C_{11} = \frac{3B + 4C'}{3} \quad (15)$$

and

$$C_{12} = \frac{3B - 2C'}{3} . \quad (16)$$

To calculate the CD Si vacancy formation energy, a $2\times2\times2$ array of 8-atom cubic unit cells are used with 63 Si atoms, where one atom is removed at a corner. To calculate the CD Si self-interstitial formation energy, an extra Si atom is added to a tetrahedral interstitial site in the 64-atom $2\times2\times2$ supercell. The structures are not relaxed in KSDFT or OFDFT; again, the point of these simulations is not to represent the real defect structure but to test transferability across a range of strains and variations in electronic structures. The point defect energies are then calculated based on Gillan's expression:[71]

$$E_{\text{defect}} = E\left(N \pm 1,1,\frac{N \pm 1}{N}\Omega \right) - \frac{N \pm 1}{N} E(N,0,\Omega) , \quad (17)$$

where $E(N,z,\Omega)$ is the total energy for a cell with volume Ω, N atoms, and z defects. The vacancy calculation corresponds to the "-" sign while the self-interstitial calculation uses the "+" sign in Eq. (16).

We performed both unreconstructed and reconstructed Si(100) surface calculations. A 9-layer unit cell containing 9 atoms (one atom per layer) and a $p(2\times1)$ geometry with 12 layers (24 atoms) were used for the unreconstructed and reconstructed surface calculations, respectively, both with 10 Å of vacuum between periodic slabs as buffer. In the latter case, the geometry was fully relaxed in KSDFT with the two middle layers fixed at their equilibrium bulk positions to mimic a semi-infinite crystal, while the OFDFT calculations employed the relaxed geometry from KSDFT and only optimized the electron density. The final surface energy, σ, is calculated by the formula:

$$\sigma = (E_{\text{slab}} - NE_0)/(2A)\,, \quad (18)$$

where E_{slab} is the total energy of the slab, E_0 is the energy per atom in the CD Si bulk equilibrium structure, N is the number of atoms in the slab, and A is the area of the periodic slab surface unit cell.

Finally, we examined nonmagnetic (M_S=0) states of diatomic molecules. The equilibrium bond length r_e, bond dissociation energy D_0, and vibrational frequency ω_e for each diatomic are calculated. Two atoms are set up in the center of a $20\times10\times10$ Å cell, aligned along the longest direction. The bond length is varied from 1.8 Å to 10 Å to determine the energy versus bond length curve. The zero point energy, r_e, and ω_e are then determined by quadratically fitting the ±0.03 Å region around the bottom of the well. The energy difference between the equilibrium bond length and the fully dissociated limit (r=10 Å) is first computed and then the zero point energy is subtracted to obtain the D_0 values.

IV. Results and Discussion

A. Bulk properties for ground state semiconductors

To test the WGCD model, we first calculate bulk equilibrium volumes (V_0), bulk moduli (B), and equilibrium energies ($E_{\min}$) for CD Si and a variety of ZB III-V semiconductors. The shift parameter m is set to zero in these calculations. We adjusted the two parameters a and b in the semilocal KEDF to match KSDFT total energies and equilibrium volumes.

Table III lists calculated bulk properties and the optimal a and b for each semiconductor ground state. The KSDFT total energies and equilibrium volumes are very well reproduced by OFDFT when a and b are tuned, but this is simply a measure of the quality of the fit. Some measure of transferability is provided by predicting bulk moduli, which also agree well with KSDFT benchmarks. Figure 5 displays total energy versus volume per atom for CD Si and per formula unit for ZB GaAs. The OFDFT curves match the KSDFT ones quite well over a considerable range. The accurate bulk properties demonstrate the validity of the WGCD model for treating semiconductor phases.

The current WGCD model has comparable accuracy to the HC KEDF for treating ground state semiconductors.[49] It shows significant improvement over the earlier re-parameterized WGC KEDF OFDFT calculations.[46] There are two parameters in the WGCD model, a and b, besides the three parameters, α, γ, and ρ_* in the original WGC KEDF. We find that the bulk properties V_0 and B hardly change when tuning these three WGC KEDF parameters while total energies are shifted slightly. Tuning γ in the range 2.2-4.0 and ρ_* in the range $1.0\rho_0$-$1.1\rho_0$ changes the total energy per atom by less than 10 meV. Tuning α in the range 0.3-0.8 also changes total energy per atom by less than 0.1 eV. Therefore, these parameters are not sensitive and we fix their values as $\alpha = (5-\sqrt{5})/6$, $\beta = 5/3 - \alpha$, and γ=3.6 in all calculations,[46] and $\rho_* = \rho_0$ in all bulk calculations. All ground state semiconductors have very similar optimal a and b parameters, with

$a \sim 0.8$ and $b \sim 0.7$ (Table III), and only small changes in V_0 and B occur when tuning these two parameters in a reasonable range (Figure 6). Increasing a while keeping b constant increases V_0 while reducing B, but both are still in reasonable agreement with KSDFT values. The total energy shifts by about 1 eV over this range of a (Figure 6). Tuning b has similar effects on the total energy but opposite effects on V_0 and B, i.e., increasing b reduces V_0 and increases B. Apparently, a rather large range of a and b parameter sets produce reasonable bulk properties though with different equilibrium total energies. In the next section, we will show that relative energies of different phases are correctly preserved compared to KSDFT benchmarks, although the energies are shifted somewhat. These facts again demonstrate that the WGCD model contains the right physics for treating semiconductor phases while the specific semilocal model describing the localized density has a smaller effect on the results.

B. KEDF Transferability

To test the transferability of our model, we next use a universal parameter set for all ground state semiconductors. Table IV shows the bulk properties computed with the average a=0.835 and b=0.679 values derived from the optimal values for different phases in Sec. A. The WGCD OFDFT bulk properties are still very close to KSDFT values. The predicted equilibrium volumes generally exhibit less than 2% error compared to KSDFT results. The maximum deviation is for InAs, +5%, corresponding to a less than 2% error in the lattice constants. The bulk moduli are also in reasonable agreement with KSDFT values. The deviation in total energies per 2-atom primitive unit cell is usually smaller than 1 eV (~0.5%), with the maximum error being 1.3 eV for CD Si. Figure 7 shows the general trend in equilibrium total energies among those ground state semiconductors. The KSDFT trend is well reproduced by OFDFT within both the new

WGCD model and the HC KEDF with universal λ and β values.[49] The WGCD absolute energies are actually in slightly better agreement with KSDFT than the HC energies.

After calculating ground state semiconductors, we next apply the WGCD model to calculate phase energy differences among other bulk Si phases. Unfortunately, using the same parameters (averaged a and b or just those optimal for CD Si, and m=0) for all phases does not yield correct phase orderings. The WGCD model successfully predicts semiconductor phases because we take special care of the localized density. However, this physics obviously becomes unsound for metallic phases, where very little localized electron density exists and therefore the density decomposition is not necessary. Although we designed the scale function such that the WGCD model recovers WGC KEDF for nearly-free-electron-like systems, Si metallic phases (cbcc through fcc in Table I) still feature considerable density variations, thus leading to the unphysical density decomposition and energetics. A better scale function which could more reasonably identify regions of localized electrons might solve this problem. However, here we simply make use of the shift parameter m. Thus, for all Si phases examined, we fix the a and b values to those optimized for CD Si and only tune m to match KSDFT phase energy differences, leaving equilibrium volumes and bulk moduli as tests of transferability.

The WGCD KEDF generally predicts excellent bulk moduli for each phase (Table V), which represents an improvement over the HC KEDF that systematically predicts too small B for metallic phases.[49] The improvement undoubtedly is due to the reliability of the WGC KEDF for metallic phases.[33] The best results for V_0 appear at both ends of the table, CD and HD on the left with low coordination numbers (4 each), and hcp, bcc, and fcc on the right with high coordination numbers (12, 8, and 12, respectively). The equilibrium volumes for these phases deviate less than 2% from the KSDFT benchmarks. CD and HD are covalently-bonded

semiconductors, so the WGCD model describes them well; the hcp, bcc, and fcc phases are the most metallic ones, so when m is large (making the WGCD KEDF nearly revert to the WGC KEDF), the properties are well predicted mainly due to the quality of the WGC KEDF. The phases with intermediate coordination numbers (middle of Table V) feature slightly increased, but still reasonable errors, up to +10% for the bct5 structure. Despite their metallic nature, these phases still exhibit comparatively large density variations, so use of the WGC KEDF is not as well founded. On the other hand, the electrons are not well localized in these phases, so the density decomposition is questionable. Adjusting the m parameter balances these two limits and produces correct phase energy differences. However, bulk properties are not very accurate.

The trend for optimal m values for each phase is clear. From the left-hand side to the right-hand side of Table V, the optimal m value gradually increases. The physical meaning behind this is also obvious; generally, more metallic phases correspond to smaller density variations and less localized electrons, which means we do not need to scale down the localized density as much as we do in semiconductor phases. Mathematically, larger m leads to smaller ζ and thus a larger value of $F(\mathbf{r})$. The small optimal m=0.03 for the HD structure lies very close to the optimal m=0 for CD Si. As the phases become mostly metallic, such as fcc Si, the optimal m value becomes as large as 0.4. The minimum value of the final self-consistent scale function in fcc Si is around 0.995, which means we hardly even need the density decomposition. As expected, the results for fcc Si are very similar to the original WGC results.[46]

We also calculate the Si CD-to-β-tin phase transition pressure. When using the same parameters (a=0.864, b=0.67, m=0) for both phases, the β-tin phase has a much lower energy than the CD phase. Consequently, the transition pressure is unphysically predicted as -12.0 GPa compared to 5.6 GPa in KSDFT. If we employ the optimal m for each phase (m=0 for CD and

m=0.114 for β-tin Si), we obtain a fairly reasonable transition pressure of 6.9 GPa, a bit larger than the KSDFT result due to a larger β-tin V_0 predicted by the WGCD model. This again illustrates the need of a more transferable scale function upon change of coordination numbers.

Besides energetics, we also verify the equilibrium structure for each phase. The CD, sc, bcc, and fcc structures feature no internal degrees of freedom while the cbcc, β-tin, and hcp structures feature one, which we scan in a wide range to find each equilibrium structure. The optimized WGCD OFDFT internal degrees of freedom for these three phases are in excellent agreement with KSDFT benchmarks (Table V). The HD and bct5 structures contain two internal degrees of freedom. When we carry out a two-dimensional scan for the *c/a* ratio and the internal coordinate x for the HD structure, the WGCD KEDF does not exhibit a global minimum. We therefore instead performed two sets of constrained minimizations in which we fixed the *c/a* ratio from KSDFT and scanned x, or vice versa. The resulting optimized *c/a* or x and the corresponding bulk properties are shown in Table V, labeled as HD1 and HD2, respectively. For both of them, the optimized values are close to KSDFT benchmarks. The bct5 structure is the most ill-behaved with the WGCD KEDF, with no minimum found in either a global two-dimensional search or one-dimensional constrained searches. In the table, the results for bct5 are calculated using the KSDFT-relaxed geometry. This shows a limitation of the current OFDFT model for geometry optimization: bond-bending is not captured properly yet within OFDFT. This issue will be discussed further in Sec. D.

We also calculated properties of various WZ III-V semiconductors, which have a similar structure to HD Si. As a transferability test, the average a and b values from CD Si and ZB III-V compounds, and the optimal value of m for HD Si were used in all WZ calculations. Similarly to HD Si, no global minimum can be found for the two degrees of freedom, the *c/a* ratio and

internal coordinate *x*. Table VI shows the results of one-dimensional constrained searches analogous to those done for HD Si. Generally the *c/a* ratio and the *x* values are fairly close to but systematically smaller than KSDFT values. Equilibrium volumes and bulk moduli are all reasonably reproduced, with the largest deviation being +6% for InAs's equilibrium volume and +15% for GaSb's bulk modulus. The phase energy differences are generally larger than KSDFT. Considering the small energy difference between these two phases, ~10 meV, the results are fairly reasonable.

C. Ground state electron density

To further test our formalism, we compare the ground state densities for CD Si and ZB GaAs calculated within OFDFT-WGCD, OFDFT-HC and KSDFT (Figure 8). Although the original WGC KEDF density is larger than the KSDFT density in the bonding region (Figure 1, leftmost density peak), the WGCD model reduces the density significantly, to the point of underestimating it (Figure 8), similar to the HC KEDF.[49] For CD Si, the maximum density is a bit smaller than the HC KEDF prediction and a dip in the density peak is exaggerated compared to KSDFT. In the non-bonding region (lower density regions between the two smaller density peaks), the WGCD density is larger than the KSDFT density, suggesting a tendency to over-delocalize the density, presumably originating in the parent WGC KEDF. For ZB GaAs, the WGCD density is again smaller than the KSDFT density though a bit larger than the HC KEDF density.[49] In this case, the asymmetric shape of the bonding peak (due to the polar covalent nature of the Ga-As bond) is exaggerated.

The parameters *a* and *b* also influence the ground state density distribution. Increasing *a* and *b* generally lowers the density in the bonding region (Figure 6, bottom panel). This makes sense

because increasing them will increase the kinetic energy contribution (aTF+bvW) of the localized electrons, making it less favorable for electrons to be there, leading to a smaller density in the bonding region. Unfortunately, we cannot simultaneously reproduce well the KSDFT V_0, B, total energy, and ground state density. To guarantee good V_0, B, and density, we have to decrease a and b substantially, leading to a total energy much lower than the KSDFT benchmark. Here, we made the total energy a priority and tolerate deviations in the ground state density (even though in principle these two quantities are of course related to each other, but use of approximate KEDFs ensures that we cannot reproduce both of them simultaneously). In cases for which an accurate ground state density is critical, parameters can be re-adjusted slightly to obtain a better density instead of a better total energy. Encouragingly, even when we use nonoptimal parameter values, such as average values that produce residual errors in total energies, the relative energy ordering is still reasonable (Table IV). Of course the $aT_{\mathrm{TF}} + bT_{\mathrm{vW}}$ KEDF is not the only option to treat the localized density. Better choices of a localized density KEDF model and scale function might improve the results and resolve this dilemma.

D. Elastic constants

In this section, we calculate elastic constants for ground state CD Si using the WGCD model. The results are listed in Table VII, along with KSDFT, HC KEDF, and WGC KEDF results for comparison. For the bulk modulus, both the HC and WGCD KEDF results are close to the KSDFT value and much better than the original WGC result. The shear moduli C_{44} and C' are more problematic because they involve bond bending. The original WGC KEDF gives wrong signs for both of them while the HC and WGCD models both give positive values for C_{44}, though still considerably smaller than KSDFT. For C', the HC result is positive while the WGCD result is still negative. However, all the OFDFT predictions of C' differ substantially

from the KSDFT benchmark. Because C_{11} and C_{12} are calculated from C_{44} and C', good results such as for the WGC C_{12} must be considered fortuitous.

OFDFT with available KEDFs clearly fails to treat bond-bending reasonably, either using the HC KEDF or the current WGCD model. Although both are able to capture some part of the right physics regarding the semiconductor linear response behavior (HC) or localized electrons (HC and WGCD), the lack of orbitals still makes describing directional deformation difficult for OFDFT. This problem is also related to the geometry optimization problem mentioned for HD and bct5 Si in Sec. B, which also involves bond bending. Some efforts have been made on the bond-bending problem in OFDFT,[78] but a more satisfactory and general solution is still needed.

E. Defect formation energies

To further test our model, we calculate the CD Si vacancy and self-interstitial formation energies and Si(100) surface energies, and compare the results to corresponding HC KEDF OFDFT and KSDFT values (Table VIII). Unfortunately, the WGCD model predicts unsatisfactorily small vacancy and very negative self-interstitial formation energies, similar to but worse than HC KEDF results.[49] The insufficient transferability of the parameter m is the likely cause; the optimal m for CD Si generates incorrect energies for local defect geometries. Again, the scale function is crucial. An ideal one will allow us to locate and separate the localized electrons reasonably and effectively not only in different structures, but also in different spatial regions in the system. The problem could very well disappear if we find a superior scale function in the future.

We then calculate the energy of the unreconstructed, unrelaxed, bulk-terminated Si(100) surface. The HC and WGCD KEDF OFDFT surface energies are both quite accurate compared

to the KSDFT benchmark (Table VIII). As is well known, the Si(100) surface reconstructs to form Si-Si bonds.[74-75] To model the actual reconstructed surface, we relaxed the Si surface with KSDFT and employ the KSDFT-relaxed geometry in OFDFT calculations for comparison. Here, the surface reconstructs to form rows of non-alternately buckled dimers (p(2x1) symmetry); we realize that alternately buckled dimers may be slightly lower in energy[72-77] but such a state requires a p(2x2) periodic unit cell, which is more expensive to simulate. Since our goal is simply to compare KSDFT to OFDFT, this p(2x1) structure is sufficient. The KSDFT reconstructed surface energy is significantly lower than the unreconstructed one. Likewise, both OFDFT models reproduce this trend, with WGCD prediction being somewhat surprisingly more accurate than the HC one.

F. Diatomic molecules

As a final test, we employ our model to calculate properties of diatomic molecules. The original WGC fails to converge for molecules whereas WGCD calculations always converge for all systems we have tried. Here we use the optimal parameters for bulk CD Si. Unlike the case of a periodic slab surface model, the choice of ρ_c is less obvious in a molecule (see Sec. III for details). We therefore employ two different ρ_c values to explore their effects. Table IX shows the results for the nonmagnetic states of various homonuclear diatomics. When ρ_c=0.005 a.u., a value similar to that used in CD Si(100) surface calculations, the spectroscopic quantities D_0 (the zero-point-corrected bond dissociation energy), r_e (the equilibrium bond length), and ω_e (the harmonic vibrational frequency) are quite well reproduced by the WGCD model for the Al family dimers compared to KSDFT benchmarks. By contrast, D_0 and ω_e are mostly badly underestimated while r_e is somewhat overestimated for Si_2 and P family dimers. Physically, the Al family dimers feature a single covalent σ bond, just as in CD Si, and therefore similar

parameters generate reasonable properties for these dimers. However, Si_2 and P family dimers are doubly or triply covalently bonded, with more localized electrons in the bonding region. The current parameters based on single σ bonds in crystals underestimate the electron localization in these multiply-bonded diatomics containing π bonds. We find that reducing ρ_c can considerably improve the results for Si_2 and P family dimers. Mathematically, smaller ρ_c leads to smaller ρ_0^{del}, larger ζ, and thus smaller $F(\mathbf{r})$, which means more localized electron density will be scaled out. For a smaller ρ_c, we now obtain very good agreement for the shape of the potential energy curve (Figure 9) and its spectroscopic parameters D_0, r_e, and ω_e (Table IX) for Si_2. However, although using a lower ρ_c improves the properties of P family dimers, the WGCD model still underestimates D_0 and ω_e while overestimating r_e values, showing that OFDFT-WGCD still cannot accurately treat triply-bonded molecules. Al family dimers are overbound with this smaller cutoff density, because electron localization is overestimated. These results again illustrate that a more transferable scale function is needed for different bonding environments.

G. Numerical efficiency

Finally, we compare the numerical efficiency of different KEDF models. The WGC, the HC and the current WGCD models all exhibit quasi-linear scaling (O(NlnN)). WGC has a small prefactor while the HC KEDF has a much larger prefactor approximately equal to the number of bins used in the interpolation,[50] which increases if density variations become significant. In the WGCD formalism, the self-consistency loop for $F(\mathbf{r})$ translates into a computational cost several (<10) times larger than a WGC KEDF calculation. However, because WGC calculations are very fast, the current model is faster than the HC KEDF, especially in large systems with considerable density variations (see Table X). As expected, for metallic phases with small density variations, the HC KEDF is only slightly slower. However, as the system becomes covalent or involves

vacuum, the HC KEDF becomes significantly more expensive than the WGCD formalism; for example, the Si(100) surface calculations are 19 times slower using the HC KEDF than the WGCD model. To simulate interesting large scale systems such as nanostructures, the new WGCD model will provide a more efficient approach while still preserving accuracy comparable to the HC KEDF for covalent materials and to the WGC KEDF for metals.

V. Conclusions

In this work, we proposed a density decomposition formalism to evaluate the kinetic energy within OFDFT, in order to treat covalent molecules and materials not only accurately but also efficiently within OFDFT. We introduced a scale function dependent on the local density to identify localized electrons and further decompose the total density into localized and delocalized densities, treating the former with a semilocal KEDF and the latter with the nonlocal WGC KEDF. There exists great flexibility in the choice of scale function. The numerically constructed one used in this work reproduces correct limits when generating delocalized electron densities. The formalism is fully self-consistent by performing another loop that guarantees a self-consistent scale function over the whole space.

We tested our model on a diverse set of covalently bonded systems, including Si, III-V semiconductors and homonuclear diatomic molecules. The bulk properties of ground state semiconductors agree well with KSDFT benchmarks when two parameters a and b (describing the TF and vW KEDF contributions) are adjusted. Even with one (average) parameter set, bulk properties as well as relative energies are generally correct, showing the good transferability of the model; moreover, the total energies are still close to KSDFT values and more accurate than the previously proposed HC KEDF in most cases. The shift parameter m in the scale function needs to be tuned to achieve correct phase energy orderings in Si. For the HD Si structure,

similar tetrahedral bonding to CD structure leads to very small adjustments, while metallic phases require larger optimal m, reducing the scaling of less localized electrons. With adjusted parameter values, our model also accurately describes metallic phases due to the accuracy of the WGC KEDF contained in the model. Numerically, the formalism stabilizes the WGC KEDF calculation and also handles systems with vacuum present in the periodic cell, such as surfaces and molecules. The Si(100) surface energies and diatomic molecule spectroscopic properties are also reasonably close to KSDFT benchmarks. The current formalism exhibits significantly higher computational efficiency than the HC KEDF, especially in cases where large density variations exist, such as surfaces and molecules. However, several defects still exist in this model. The density in the bonding region is underestimated. It can be improved via tuning parameters but this sacrifices the accuracy of other properties like total energies. Furthermore, the WGCD model fails to predict a reasonable CD to β-tin phase transition unless different optimal parameters are used for each phase, the vacancy formation energy is underestimated, and the self-interstitial formation energy even has the wrong sign. All of these failures are related to the less-than-satisfactory transferability of the model between different bonding environments. Finally, the current OFDFT model still has difficulty describing bond bending and directional deformation correctly, as demonstrated by poorly predicted C_{44} and C', especially for C' (with the wrong sign). The failure to find a global minimum when optimizing HD and bct5 structures is also related to this problem.

A better scale function could crucially improve the quality of the current model. As stated earlier, ideally we would hope the scale function could help us determine where and how many localized electrons should be scaled and where the system has only delocalized electrons so that the WGC KEDF can be used there. At present, although the density decomposition

captures part of the correct physics of covalent systems, the scale function is clearly not perfect, with plenty of room for future improvement. For a superior scale function, we can consider making use of information beyond just the density, such as density gradients or the Laplacian. Recent studies probing the relation between density distributions and bonding properties could prove useful.[79, 80] Moreover, the models to describe the localized, interaction, and delocalized kinetic energies are also flexible and improvable.

Acknowledgements

We are grateful to Dr. Youqi Ke, Dr. Florian Libisch, Dr. Chen Huang, and Ilgyou Shin for helpful discussions. We thank the Office of Naval Research and the National Science Foundation for their support of this research.

References

1. P. Hohenberg and W. Kohn, Phys. Rev. **136**, B864 (1964).

2. W. Kohn and L. J. Sham, Phys. Rev. **140**, A1133 (1965).

3. J. M. Soler, E. Artacho, J. D. Gale, A. García, J. Junquera, P. Ordejón and D. Sánchez-Portal, J. Phys.: Condens. Matter **14**, 2745-2779 (2002).

4. C. K. Skylaris, P. D. Haynes, A. A. Mostofi, and M. C. Payne, J. Chem. Phys. **122**, 084119 (2005).

5. M. J. Gillan, D. R. Bowler, A. S. Torralba, T. Miyazaki, Comput. Phys. Commun. **177**, 14 (2007).

6. D. R. Bowler and T. Miyazaki, Rep. Prog. Phys. **75**, 036503 (2012).

7. D. R. Bowler, J. L. Fattebert, M. J. Gillan, P. D. Haynes, and C. K. Skylaris, J. Phys.: Condens. Matter **20**, 290301 (2008).

8. W. Kohn, Phys. Rev. Lett. **76**, 3168 (1996).

9. S. Goedecker, Rev. Mod. Phys. **71**, 1085 (1999).

10. S. Ismail-Beigi, T. A. Arias, Phys. Rev. Lett. **82**, 2127 (1999).

11. F. Shimojo, R. K. Kalia, A. Nakano, K. Nomura, P. Vashishta, J. Phys.: Condens. Matter **20**, 294204 (2008).

12. A. Nakano, R. K. Kalia, K. Nomura, et al., Int. J. High Perform. Comput. Appl. **22,** 113 (2008).

13. Y. A. Wang and E. A. Carter, in Theoretical Methods in Condensed Phase Chemistry, edited by S. D. Schwartz (Kluwer, Dordrecht, 2000), p. 117.

14. G. Ho, V. L. Ligneres, and E. A. Carter, Comput. Phys. Commun. **179**, 839 (2008).

15. L. Hung and E. A. Carter, Chem. Phys. Lett. **475**, 163 (2009).

16. I. Shin, A. Ramasubramaniam, C. Huang, L. Hung, and E. A. Carter, Philos. Mag. **89**, 3195 (2009).

17. Q. Peng, X. Zhang, L. Hung, E. A. Carter, and G. Lu, Phys. Rev. B **78**, 054118 (2008).

18. L. Hung and E. A. Carter, J. Phys. Chem. **115**, 6269 (2011).

19. G. Ho and E. A. Carter, J. Comput. Theor. Nanos. **6**, 1236 (2009).

20. L. Hung and E. A. Carter, Modell. Simul. Mater. Sci. Eng. **19**, 045002 (2011).

21. I. Shin and E. A. Carter, Modell. Simul. Mater. Sci. Eng. **20**, 015006 (2011).

22. N. Choly, G. Lu, W. E, and E. Kaxiras, Phy. Rev. B **71**, 094101 (2005).

23. X. Zhang and G. Lu, Phy. Rev. B **76**, 245111 (2007).

24. L. H. Thomas, Proc. Cambridge Philos. Soc. **23**, 542 (1927).

25. E. Fermi, Rend. Accad. Naz. Lincei **6**, 602 (1927).

26. E. Fermi, Z. Phys. **48**, 73 (1928).

27. C. F. von Weizsäcker, Z. Phys. **96**, 431 (1935).

28. E. Chacón, J. E. Alvarellos, and P. Tarazona, Phys. Rev. B **32**, 7868 (1985).

29. P. García-González, J. E. Alvarellos, and E. Chacón, Phys. Rev. B **53**, 9509 (1996).

30. P. García-González, J. E. Alvarellos, and E. Chacón, Phys. Rev. B **57**, 4857 (1998).

31. L. W. Wang and M. P. Teter, Phys. Rev. B **45**, 13196 (1992).

32. Y. A. Wang, N. Govind, and E. A. Carter, Phys. Rev. B **58**, 13465 (1998); **64**, 129901-1(E) (2001).

33. Y. A. Wang, N. Govind, and E. A. Carter, Phys. Rev. B **60**, 16350 (1999); **64**, 089903(E) (2001).

34. F. Perrot, J. Phys.: Condens. Matter **6**, 431 (1994).

35. M. Pearson, E.Smargiassi, and P. A. Madden, J. Phys.: Condens. Matter **5**, 3321 (1993).

36. E. Smargiassi and P. A. Madden, Phys. Rev. B **49**, 5220 (1994).

37. E. Smargiassi and P. A. Madden, Phys. Rev. B **51**, 117 (1995).

38. N. W. Ashcroft and N. D. Mermin, Solid State Physics (Holt Rinehart & Winston, Philadelphia, 1976).

39. W. A. Harrison, Solid State Theory (Dover, New York, 1980).

40. M. Foley and P. A. Madden, Phys. Rev. B **53**, 10 589 (1996).

41. B. J. Jesson, M. Foley, and P. A. Madden, Phys. Rev. B **55**, 4941 (1997).

42. E. Smargiassi and P. A. Madden, Phys. Rev. B **51**, 117 (1995).

43. K. M. Carling and E. A. Carter, Modell. Simul. Mater. Sci. Eng. **11**, 339 (2003).

44. G. Ho, M. T. Ong, K. J. Caspersen, and E. A. Carter, Phys. Chem. Chem. Phys. **9**, 4951 (2007).

45. G. Ho, C. Huang, and E. A. Carter, Curr. Opin. Solid State Mater. Sci. **11**, 57 (2008).

46. B. Zhou, V. L. Ligneres, and E. A. Carter, J. Chem. Phys. **122**, 044103 (2005).

47. B. Zhou and E. A. Carter, J. Chem. Phys. **122**, 184108 (2005).

48. V. Ligneres, Ph.D. thesis, Princeton University, 2008.

49. C. Huang and E. A. Carter, Phys. Rev. B **81**, 045206 (2010).

50. C. Huang and E. A. Carter, Phys. Rev. B **85**, 045126 (2012).

51. Y. Ke, F. Libisch, J. Xia, L. –W. Wang, and E. A. Carter, to be published.

52. J. Xia, C. Huang, I. Shin, and E. A. Carter, J. Chem. Phys. **136**, 084102 (2012).

53. T. A.Wesolowski and A.Warshel, J. Phys. Chem. **97**, 8050 (1993).

54. T. A. Wesolowski, H. Chermette and J. Weber, J. Chem. Phys. **105**, 9182 (1996).

55. T. A. Wesolowski, J. Chem. Phys. **106**, 8516 (1997).

56. J. M. G. Lastra, J. W. Kaminski, and T. A. Wesolowski, J. Chem. Phys. **129**, 074107 (2008).

57. G. Senatore and K. R. Subbaswamy, Phys. Rev. B **34**, 5754 (1986).

58. N. Govind, Y. A. Wang, A. J. R. da Silva, and E. A. Carter, Chem. Phys. Lett. **295**, 129 (1998).

59. N. Govind, Y. A. Wang, and E. A. Carter, J. Chem. Phys. **110**, 7677 (1999).

60. B. Silvi and A. Savin, Nature **371**, 683 (1994).

61. A. D. Becke and K. E. Edgecombe, J. Chem. Phys. **92**, 5397 (1990).

62. L. Hung, C. Huang, I. Shin, G. Ho, V. L. Ligneres, and E. A. Carter, Comput. Phys. Comm. **181**, 2208 (2010).

63. X. Gonze, J.-M. Beuken, R. Caracas, F. Detraux, M. Fuchs, G.-M. Rignanese, L. Sindic, M. Verstraete, G. Zerah, F. Jollet, M. Torrent, A. Roy, M. Mikami, Ph. Ghosez, J.-Y. Raty, and D. C. Allan, Comput. Mater. Sci. **25**, 478 (2002).

64. D. M. Ceperley and B. J. Alder, Phys. Rev. Lett. **45**, 566 (1980).

65. J. P. Perdew and A. Zunger, Phys. Rev. B **23**, 5048 (1981).

66. B. Zhou, Y.A. Wang, and E.A. Carter, Phys. Rev. B **69**, 125109 (2004).

67. C. Huang and E. A. Carter, Phys. Chem. Chem. Phys. **10**, 7109 (2008).

68. H. J. Monkhorst and J. D. Pack, Phys. Rev. B **13**, 5188 (1976).

69. F. D. Murnaghan, Proc, Natl, Acad. Sci. U. S. A. **30**, 244 (1944).

70. S. Q. Wang and H. Q. Ye, J. Phys.: Condens. Matter **15**, 5307 (2003).

71. M. J. Gillan, J. Phys.: Condens. Matter **1**, 689 (1989).

72. M. J. Cardillo and G. E. Becker, Phys. Rev. Lett. **40**, 1148 (1978).

73. M. J. Cardillo and G. E. Becker, Phys. Rev. B **21**, 1497 (1980).

74. R. J. Hamers, R. M. Tromp and J. E. Demuth, Phys. Rev. B **34**, 5343 (1986).

75. D. Haneman, Rep. Prog. Phys. **50**, 1045 (1987).

76. R. A. Wolkow, Phys. Rev. Lett. **68**, 2636 (1992).

77. P. C. Weakliem, G. W. Smith, and E. A. Carter, Surface Sci. Lett. **232**, L219 (1990).

78. C. Huang, Ph.D. thesis, Princeton University, 2011.

79. H. J. Bohórquez and R. J. Boyd, Theor. Chem. Acc. **127**, 393 (2010).

80. J. Contreras-García, E. R. Johnson, S. Keinan, R. Chaudret, J.-P. Piquemal, D. N. Beratan, W. Yang, J. Chem. Theory Comput. **7**, 625 (2011).

Supplementary material

Here we provide numerical details for the scale function $f(\rho_{\text{total}}/\rho_0^{\text{del}})$ used in all the OFDFT calculations in this paper. $f(\rho_{\text{total}}/\rho_0^{\text{del}})$ values are tabulated (Table SI) and then interpolated in our code to calculate the scale function for any given $\rho_{\text{total}}/\rho_0^{\text{del}}$ value.

Tables

Table I. Ratio of maximum density to average density for different structures at their equilibrium volumes, as calculated by KSDFT. The first nine structures are for Si, where the first two are semiconducting phases and the rest are metallic.

phase	**CD**	**HD**	**cbcc**	***β*-tin**	**bct5**	**sc**	**hcp**	**bcc**	**fcc**	**Al fcc**	**Mg hcp**
ρ_{max}/ρ_0	2.835	2.836	2.497	1.748	2.362	1.733	1.423	1.489	1.441	1.180	1.210

Table II. k-point meshes and Fermi-Dirac smearing widths used in various KSDFT calculations in this work. The number of atoms in each calculation is listed in parentheses.

Systems	**k-point mesh**	E_{smear} **(eV)**
CD (2), HD (4) Si **ZB (2), WZ (4) III-V semiconductors** **Elastic constants in CD Si (2)**	12 12 12	0.0
Point defects in CD Si **(63 for vacancy; 65 for self-interstitial)**	4 4 4	0.0
cbcc (8) Si	12 12 12	0.1
***β*-tin (2), bct5 (2), sc (1), hcp (2), bcc (1), and fcc (1) Si**	20 20 20	0.1
Unreconstructed Si(100) surface energy (9)	12 12 1	0.0
Reconstructed Si(100) surface energy (24)	6 12 1	0.0

Table III. The equilibrium volumes (V_0), bulk moduli (B), equilibrium total energies (E_{min}) per 2-atom primitive unit cell for CD Si and various ZB III-V semiconductors, and the optimal values for WGCD KEDF parameters a and b for each phase. The corresponding KSDFT results are listed in parentheses.

	V_0 (Å^3)	B (GPa)	E_{min} (eV)	a	b
Si	39.627 (39.549)	98 (99)	-219.253 (-219.258)	0.864	0.670
AlP	40.407 (40.638)	94 (91)	-240.165 (-240.182)	0.822	0.699
AlAs	45.098 (43.620)	84 (80)	-232.909 (-232.908)	0.840	0.656
AlSb	55.665 (56.600)	60 (59)	-206.607 (-206.606)	0.840	0.677
GaP	37.741 (37.649)	80 (88)	-243.069 (-243.080)	0.847	0.655
GaAs	40.789 (40.633)	80 (75)	-235.790 (-235.799)	0.823	0.732
GaSb	52.341 (52.483)	64 (57)	-209.705 (-209.697)	0.865	0.629
InP	46.992 (46.035)	70 (73)	-235.697 (-235.722)	0.810	0.700
InAs	51.259 (49.121)	67 (65)	-228.544 (-228.537)	0.813	0.703
InSb	63.699 (62.904)	49 (50)	-202.382 (-202.387)	0.830	0.668

Table IV. Equilibrium volumes (V_0), bulk moduli (B), and equilibrium total energies (E_{min}) per 2-atom primitive unit cell for CD Si and various ZB III-V semiconductors computed with WGCD KEDF parameters set to a=0.835 and b=0.679 (averaged values from Table III). KSDFT results are given in parentheses.

	V_0 (Å^3)	B (GPa)	E_{min} (eV)
Si	39.450 (39.549)	105 (99)	-220.561 (-219.258)
AlP	40.654 (40.638)	95 (91)	-239.836 (-240.182)
AlAs	44.820 (43.620)	90 (80)	-232.749 (-232.908)
AlSb	55.657 (56.600)	56 (59)	-206.788 (-206.606)
GaP	37.426 (37.649)	90 (88)	-243.282 (-243.080)
GaAs	41.581 (40.633)	72 (75)	-236.111 (-235.799)
GaSb	51.591 (52.483)	66 (57)	-210.287 (-209.697)
InP	47.404 (46.035)	69 (73)	-234.723 (-235.722)
InAs	51.732 (49.121)	64 (65)	-227.837 (-228.537)
InSb	63.520 (62.904)	51 (50)	-202.026 (-202.387)

Table V. Equilibrium volumes (V_0), bulk moduli (B), and equilibrium total energies (E_{min}) per atom for various Si phases. The WGCD KEDF parameters a=0.864 and b=0.670 optimal for CD Si are used for all phases. The optimal scale function parameter m and the coordination number (c.n.) are also listed for each phase. The optimized internal coordinate x for cbcc and the optimized c/a ratios for β-tin and hcp structures are given. For the HD1 structure, the optimal c/a ratio is given for the internal coordinate x fixed at the KSDFT optimized value; for the HD2 structure, the optimal x value is given for the c/a ratio fixed at the KSDFT optimum. The KSDFT-relaxed bct5 structure is used in OFDFT calculations. The corresponding KSDFT benchmarks are listed in parentheses.

phase	**CD**	**HD1**	**HD2**	**cbcc**	***β*-tin**	**bct5**	**sc**	**hcp**	**bcc**	**fcc**
m	0.000	0.030	0.030	0.070	0.114	0.210	0.190	0.335	0.230	0.400
V_0 **(Å^3)**	19.821 (19.775)	19.875 (19.641)	19.897 (19.641)	18.574 (17.512)	15.992 (14.655)	18.627 (16.911)	16.908 (15.471)	14.279 (14.131)	14.309 (14.619)	14.011 (14.365)
B **(GPa)**	98 (99)	96 (100)	102 (100)	94 (102)	113 (121)	92 (97)	115 (112)	94 (92)	102 (98)	86 (82)
E_{min} **(eV)**	-109.627 (-109.629)	0.013 (0.014)	0.015 (0.023)	0.153 (0.153)	0.163 (0.167)	0.225 (0.213)	0.234 (0.235)	0.347 (0.336)	0.359 (0.352)	0.360 (0.381)
c/a **or** ***x***	-	1.56 (1.64)	0.061 (0.062)	0.204 (0.205)	0.26 (0.28)	KSDFT's geometry	-	1.66 (1.66)	-	-
c.n.	4	4	4	4	6	5	6	12	8	12

Table VI. Equilibrium volumes (V_0) and bulk moduli (B) for HD Si and various WZ III-V semiconductors. The energy differences between ground state ZB (CD for Si) and WZ (HD for Si) structures (ΔE) per formula unit (per 2-atom for Si) are also given. The WGCD KEDF parameters a=0.835 and b=0.679 (averaged values from Table III) are used. The optimal m=0.03 for HD Si in Table V is used for all phases. On the left, optimal internal coordinates x from KSDFT are used and optimal c/a ratios are listed; on the right, optimal c/a ratios from KSDFT are used and optimal x values are given. See text for details. The corresponding KSDFT benchmarks are listed in parentheses.

	c/a	V_0 (Å^3)	B (GPa)	ΔE (meV)	x	V_0 (Å^3)	B (GPa)	ΔE (meV)
Si	1.55	39.653	98	21	0.061	39.653	106	33
	(1.64)	(39.282)	(100)	(27)	(0.062)	(39.282)	(100)	(27)
AlP	1.57	41.052	95	49	0.062	40.956	89	12
	(1.64)	(40.619)	(91)	(8)	(0.063)	(40.619)	(91)	(8)
AlAs	1.57	45.184	79	43	0.062	45.148	82	55
	(1.65)	(43.603)	(80)	(11)	(0.063)	(43.603)	(80)	(11)
AlSb	1.58	56.210	61	40	0.062	56.159	62	50
	(1.65)	(56.551)	(59)	(13)	(0.063)	(56.551)	(59)	(13)
GaP	1.56	37.847	92	54	0.062	37.803	98	68
	(1.65)	(37.623)	(88)	(17)	(0.063)	(37.623)	(88)	(17)
GaAs	1.56	41.998	75	47	0.062	41.956	77	61
	(1.65)	(40.610)	(75)	(19)	(0.063)	(40.610)	(75)	(19)
GaSb	1.57	52.059	64	45	0.062	51.996	66	56
	(1.65)	(52.422)	(57)	(17)	(0.063)	(52.422)	(57)	(17)
InP	1.55	47.667	69	26	0.061	47.578	70	40
	(1.64)	(46.023)	(73)	(4)	(0.063)	(46.023)	(73)	(4)
InAs	1.56	52.122	64	26	0.061	52.056	63	39
	(1.64)	(49.115)	(65)	(6)	(0.063)	(49.115)	(65)	(6)
InSb	1.58	64.005	47	29	0.062	63.922	52	38
	(1.65)	(62.887)	(50)	(11)	(0.063)	(62.887)	(50)	(11)

Table VII. Bulk modulus (B), C_{11}, C_{12}, C_{44}, and shear modulus (C') for CD Si calculated by KSDFT and OFDFT with the HC KEDF, the WGC KEDF, and the current WGCD KEDF model. In the WGC KEDF calculations, default parameter values are used; see text for details. In the HC KEDF calculations, λ=0.01 and β=0.65 optimal for CD Si are employed. In the WGCD KEDF, a=0.864, b=0.670 and m=0 optimal for CD Si are used.

CD Si	B (GPa)	C_{11} (GPa)	C_{12} (GPa)	C_{44} (GPa)	C' (GPa)
KSDFT	99	163	66	102	49
OFDFT/HC	95	101	92	81	5
OFDFT/WGC	53	3	78	-150	-38
OFDFT/WGCD	98	89	103	52	-7

Table VIII. CD Si vacancy (E_{vf}) and self-interstitial (E_{isv}) formation energies, and surface energies (σ) for unreconstructed and reconstructed Si(100) surfaces computed by KSDFT and OFDFT with the HC KEDF and WGCD models. In HC KEDF calculations, λ=0.01 and β=0.65 optimal for CD Si are employed. In WGCD calculations, parameters optimal for bulk CD Si are used. See text for details. In surface calculations, the density cutoff ρ_c in calculating average densities is set to 6.84×10^{-3} a.u., which is the minimum density of bulk CD Si at its equilibrium volume.

	E_{vf} (eV)	E_{isv} (eV)	Un-reconstructed σ (J/m^2)	reconstructed σ (J/m^2)
KSDFT	3.31	3.37	2.273	1.196
OFDFT/HC	2.69	-1.91	2.441	1.898
OFDFT/WGCD	1.33	-6.27	2.398	1.052

Table IX. Comparison of WGCD OFDFT and KSDFT bond dissociation energies (D_0), equilibrium bond lengths (r_e), and vibrational frequencies (ω_e) for nonmagnetic Al_2, Ga_2, In_2, Si_2, P_2, As_2, and Sb_2. In all OFDFT calculations, a=0.864, b=0.670, and m=0 optimal for bulk CD Si are used. Two ρ_c values, 5×10^{-3} a.u. and 5×10^{-5} a.u. are used for comparison; see text for details. KSDFT values are given in parentheses.

dimer	D_0 (eV)	r_e (Å)	ω_e (cm^{-1})	D_0 (eV)	r_e (Å)	ω_e (cm^{-1})
	$\rho_c = 5\times10^{-3}$ a.u.			$\rho_c = 5\times10^{-5}$ a.u.		
Al_2	1.68 (1.74)	2.576 (2.473)	332 (346)	2.85 (1.74)	2.528 (2.473)	346 (346)
Ga_2	1.81 (1.69)	2.417 (2.323)	214 (212)	2.94 (1.69)	2.371 (2.323)	216 (212)
In_2	1.38 (1.64)	2.817 (2.633)	133 (157)	2.53 (1.64)	2.742 (2.633)	143 (157)
Si_2	2.87 (4.59)	2.305 (2.284)	435 (501)	4.22 (4.59)	2.281 (2.284)	482 (501)
P_2	4.14 (9.54)	2.152 (1.942)	511 (790)	5.59 (9.54)	2.137 (1.942)	586 (790)
As_2	3.40 (8.35)	2.274 (2.032)	301 (459)	4.84 (8.35)	2.247 (2.032)	327 (459)
Sb_2	2.47 (6.65)	2.731 (2.431)	210 (283)	3.97 (6.65)	2.685 (2.431)	233 (283)

Table X. Ratios of entire computational wall time of the HC KEDF to the new WGCD model for bulk fcc, cbcc, and CD Si, as well as CD Si vacancy, reconstructed Si(100) surface, and Si_2 calculations. In both HC KEDF and WGCD calculations, total energies are converged to 1 meV/atom with respective to plane wave basis kinetic energy cutoff and the binning ratio (which determines the accuracy of the interpolation method) in the HC KEDF.

	fcc	cbcc	CD	Vacancy	Surface	Si_2
t_{HC}/t_{WGCD}	3	4	5	10	19	59

Table SI. Table of $f(\rho_{\text{total}}/\rho_0^{\text{del}})$ values used for interpolation in the code.

$\rho_{\text{total}}/\rho_0^{\text{del}}$	$f(\rho_{\text{total}}/\rho_0^{\text{del}})$	$\rho_{\text{total}}/\rho_0^{\text{del}}$	$f(\rho_{\text{total}}/\rho_0^{\text{del}})$	$\rho_{\text{total}}/\rho_0^{\text{del}}$	$f(\rho_{\text{total}}/\rho_0^{\text{del}})$	$\rho_{\text{total}}/\rho_0^{\text{del}}$	$f(\rho_{\text{total}}/\rho_0^{\text{del}})$
0	0.99941176	2.5	0.45777778	5	0.24794744	7.5	0.16657338
0.1	0.99941176	2.6	0.44230769	5.1	0.24328774	7.6	0.16439136
0.2	0.99941176	2.7	0.42798354	5.2	0.23878745	7.7	0.16226505
0.3	0.99941176	2.8	0.41468254	5.3	0.23443948	7.8	0.16019241
0.4	0.99941171	2.9	0.40229885	5.4	0.23023710	7.9	0.15817148
0.5	0.99941143	3	0.39074074	5.5	0.22617387	8	0.15620041
0.6	0.99940953	3.1	0.37992832	5.6	0.22224369	8.1	0.15427740
0.7	0.99939688	3.2	0.36979167	5.7	0.21844074	8.2	0.15240076
0.8	0.99931250	3.3	0.36026936	5.8	0.21475948	8.3	0.15056887
0.9	0.99875000	3.4	0.35130719	5.9	0.21119466	8.4	0.14878017
1	0.99500000	3.5	0.34285714	6	0.20774127	8.5	0.14703319
1.1	0.97000000	3.6	0.33472333	6.1	0.20439457	8.6	0.14532650
1.2	0.89375000	3.7	0.32689395	6.2	0.20115003	8.7	0.14365875
1.3	0.82923077	3.8	0.31935812	6.3	0.19800336	8.8	0.14202864
1.4	0.77392857	3.9	0.31210481	6.4	0.19495048	8.9	0.14043492
1.5	0.72600000	4	0.30512297	6.5	0.19198750	9	0.13887641
1.6	0.68406250	4.1	0.29840163	6.6	0.18911074	9.1	0.13735197
1.7	0.64705882	4.2	0.29193001	6.7	0.18631668	9.2	0.13586051
1.8	0.61419753	4.3	0.28569754	6.8	0.18360200	9.3	0.13440097
1.9	0.58479532	4.4	0.27969397	6.9	0.18096351	9.4	0.13297235
2	0.55833333	4.5	0.27390936	7	0.17839820	9.5	0.13157369
2.1	0.53439153	4.6	0.26833411	7.1	0.17590319	9.6	0.13020407
2.2	0.51262626	4.7	0.26295898	7.2	0.17347575	9.7	0.12886259
2.3	0.49275362	4.8	0.25777510	7.3	0.17111327	9.8	0.12754841
2.4	0.47453704	4.9	0.25277397	7.4	0.16881327	9.9	0.12626071

Figures

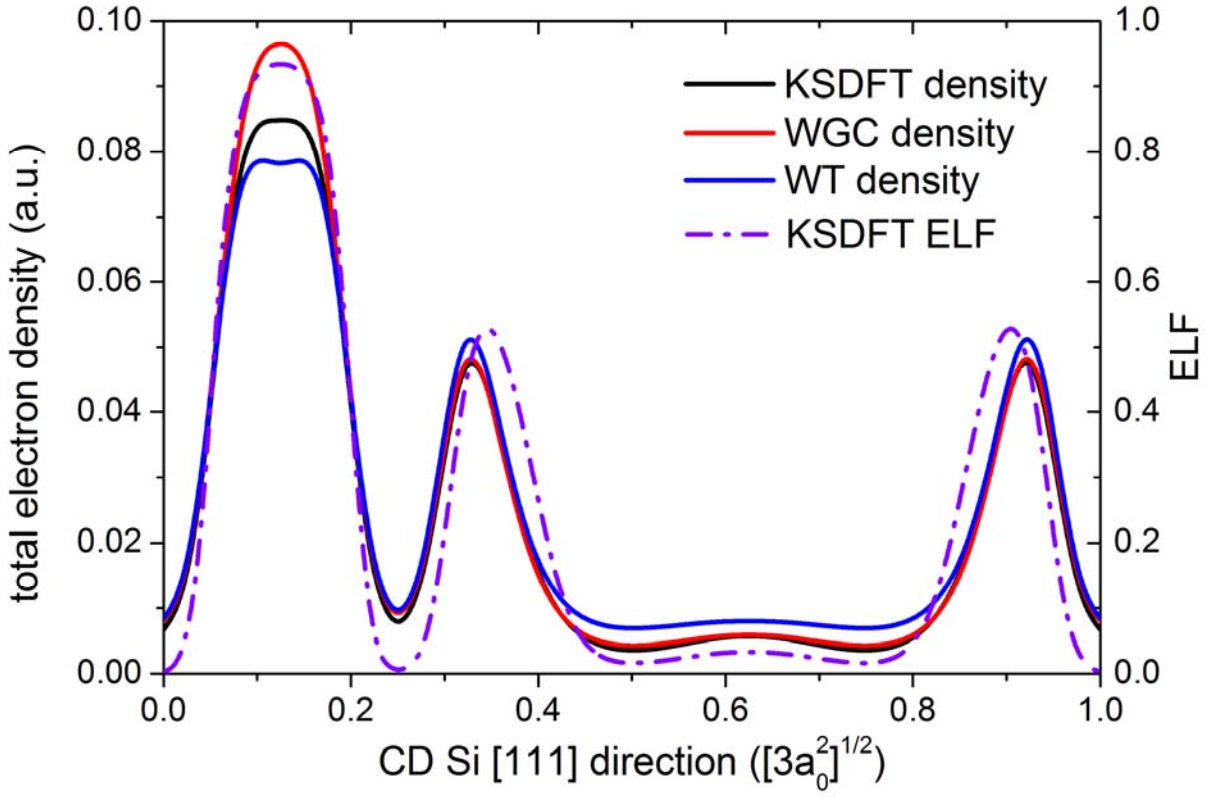

Figure 1. Self-consistent ground state electron density along the [111] direction of CD Si at its KSDFT equilibrium volume, as obtained by KSDFT, or OFDFT with either the WGC KEDF or the WT KEDF. In the WGC KEDF OFDFT calculations, the parameters α=(5-5$^{1/2}$)/6, β=(5+5$^{1/2}$)/6, γ=3.6, and $\rho_* = \rho_0$ are used. In the WT KEDF, the parameters α=β=5/6 are employed. The KSDFT electron localization function (ELF) is also plotted. The horizontal axis is normalized by $(3a_0^2)^{1/2}$, where a_0 is the KSDFT equilibrium lattice constant.

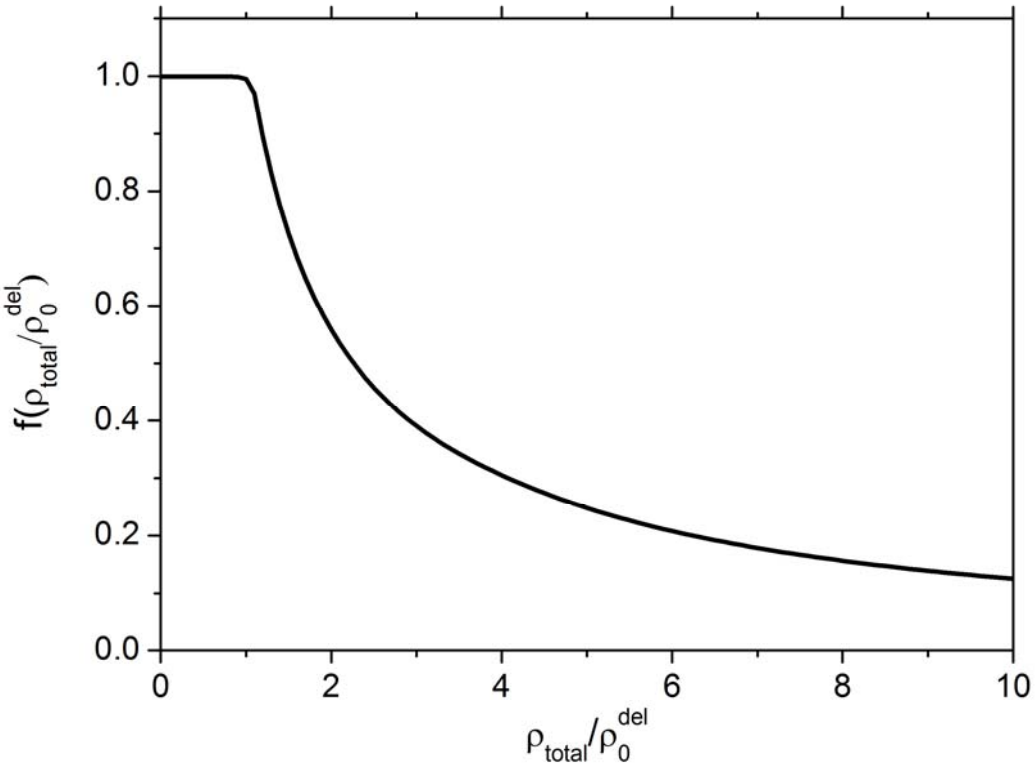

Figure 2. Numerically constructed scale function $f(\rho_{\text{total}} / \rho_0^{\text{del}})$, where ρ_0^{del} is the average delocalized density.

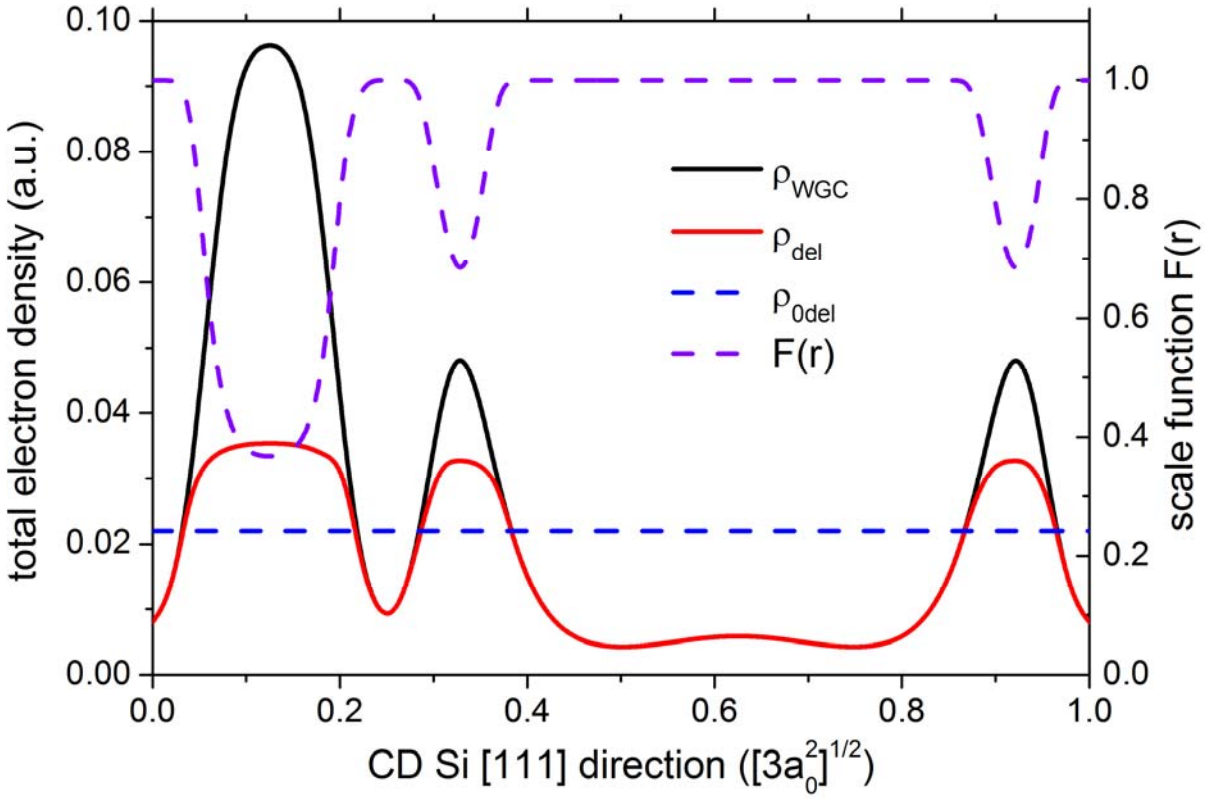

Figure 3. The self-consistent WGC density ρ_{WGC}, the scale function $f(\rho_{\mathrm{WGC}}/\rho_0^{\mathrm{del}})$, and the decomposed delocalized density $\rho_{\mathrm{del}} = \rho_{\mathrm{WGC}} \cdot f(\rho_{\mathrm{WGC}}/\rho_0^{\mathrm{del}})$ along the [111] direction as well as the average delocalized density ρ_0^{del} in CD Si at the KSDFT equilibrium volume after the first iteration. The horizontal axis is normalized by $(3a_0^2)^{1/2}$, where a_0 is the KSDFT equilibrium lattice constant.

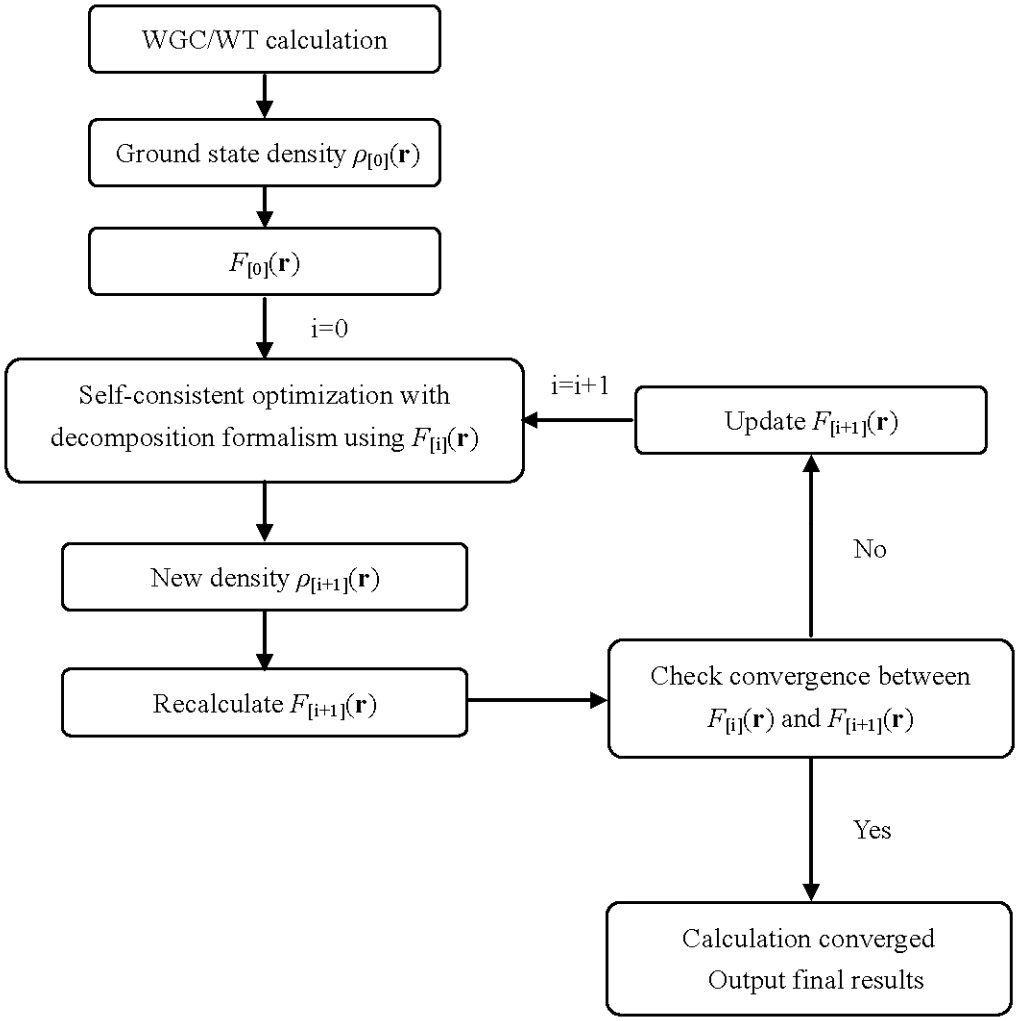

Figure 4. Flowchart of the fully-self-consistent density decomposition formalism. The subscript in square brackets represents the iteration step.

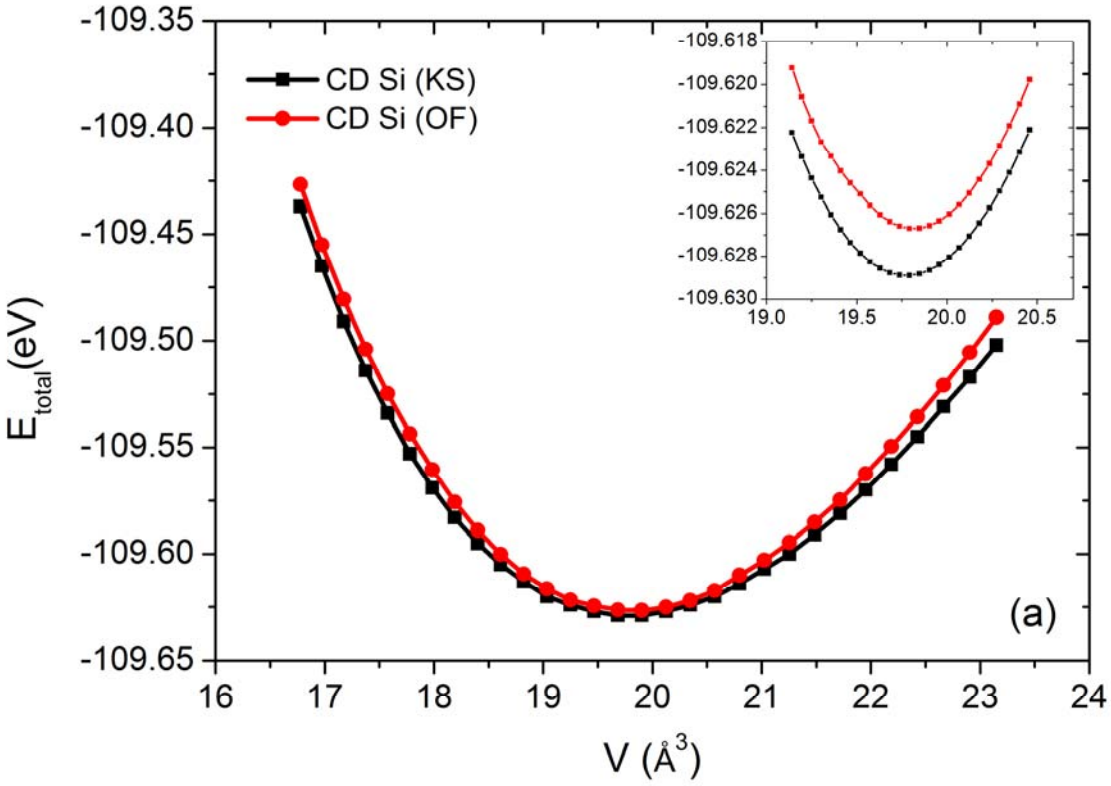
CD Si (KS)
CD Si (OF)
(a)
E_{total}(eV)
V (Å^3)
-109.35
-109.40
-109.45
-109.50
-109.55
-109.60
-109.65
16
17
18
19
20
21
22
23
24
-109.618
-109.620
-109.622
-109.624
-109.626
-109.628
-109.630
19.0
19.5
20.0
20.5

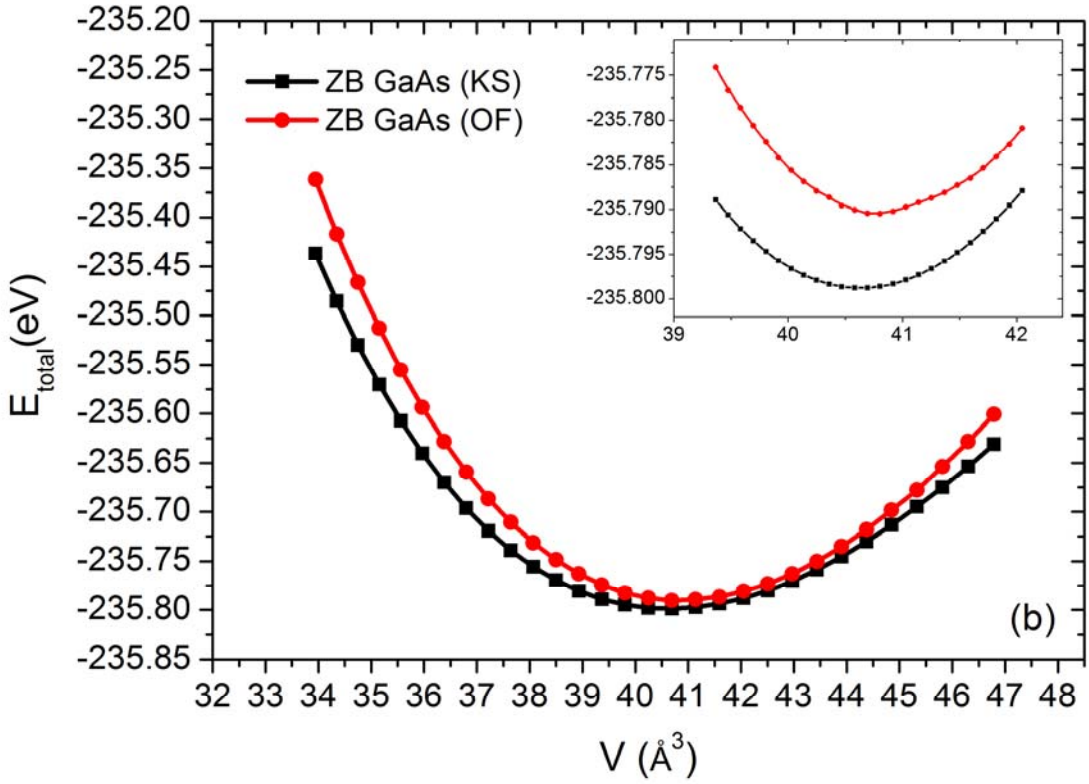

Figure 5. KSDFT and OFDFT-WGCD total energy versus volume curves (a) per atom for CD Si; (b) per formula unit for ZB GaAs. Insets show region near minimum. In OFDFT calculations, a=0.864, b=0.67 and m=0 are used for CD Si; a=0.823, b=0.732 and m=0 are used for ZB GaAs.

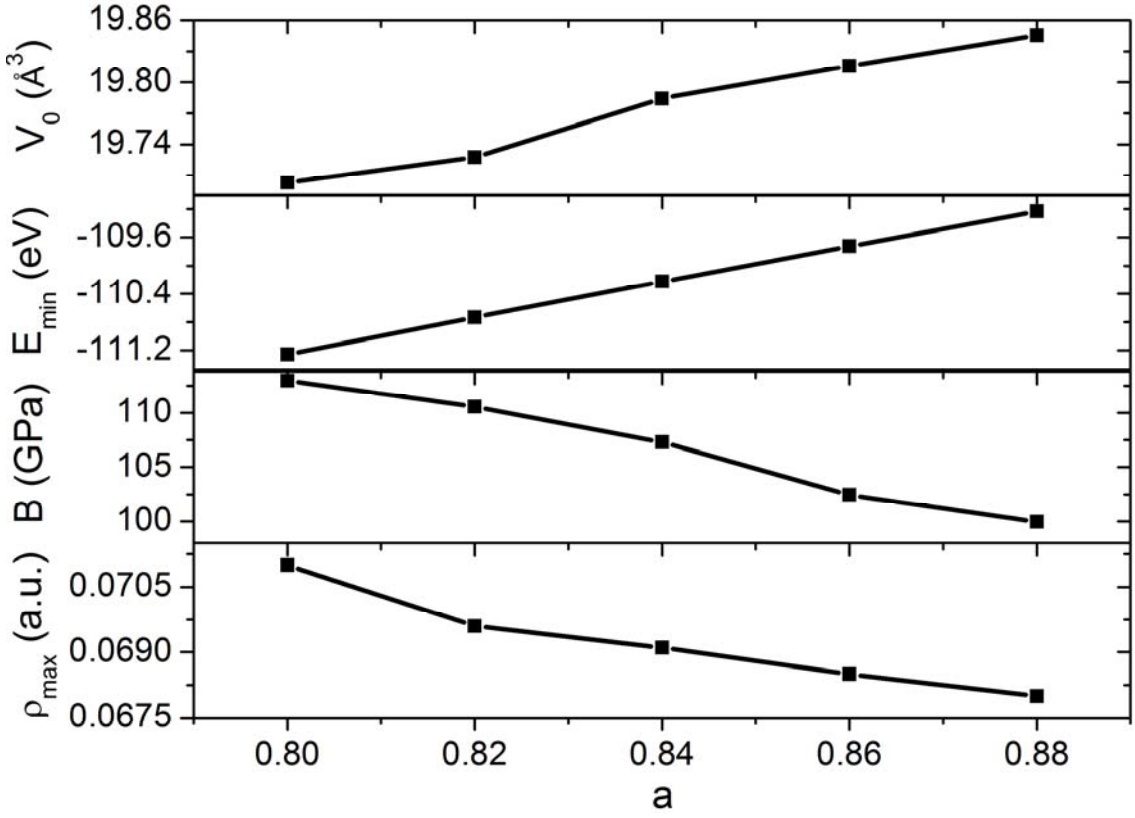

Figure 6. Variation of equilibrium volume (V_0), equilibrium total energy per atom (E_{min}), bulk modulus (B), and the maximum density at V_0 for CD Si with different values of parameter a. Parameter b is fixed as 0.670.

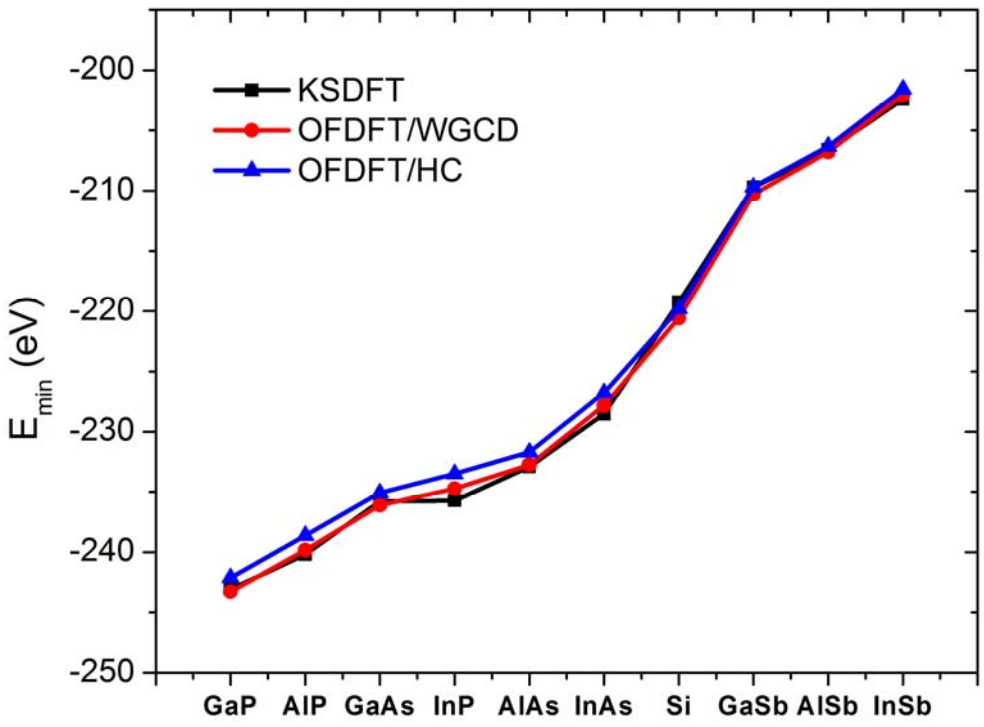

Figure 7. Total energies per 2-atom primitive unit cell for CD Si and various ZB III-V semiconductors calculated by KSDFT and by OFDFT with the HC KEDF and the WGCD model. The HC KEDF results are taken from previous literature.[49] In the WGCD calculations, the averaged values a=0.835 and b=0.679 are used, with m=0.

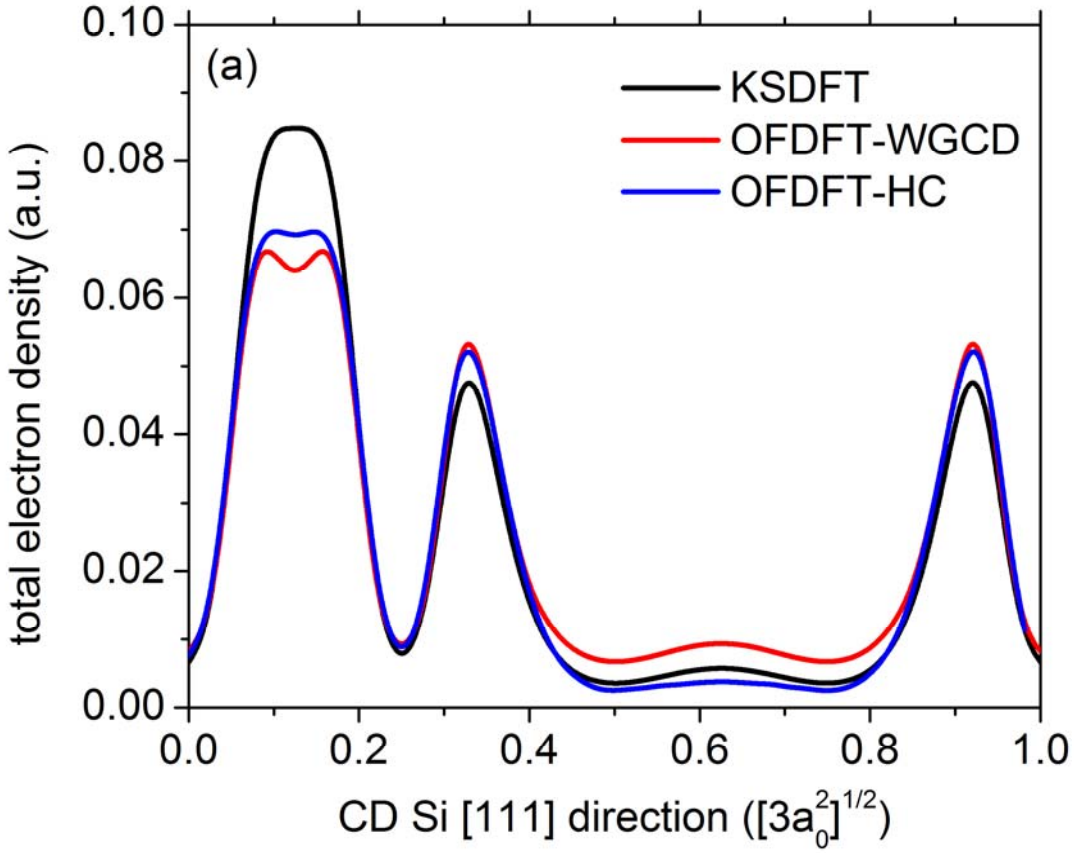
(a)
KSDFT
OFDFT-WGCD
OFDFT-HC
total electron density (a.u.)
0.10
0.08
0.06
0.04
0.02
0.00
0.0
0.2
0.4
0.6
0.8
1.0
CD Si [111] direction ([3a$_0^2$]$^{1/2}$)

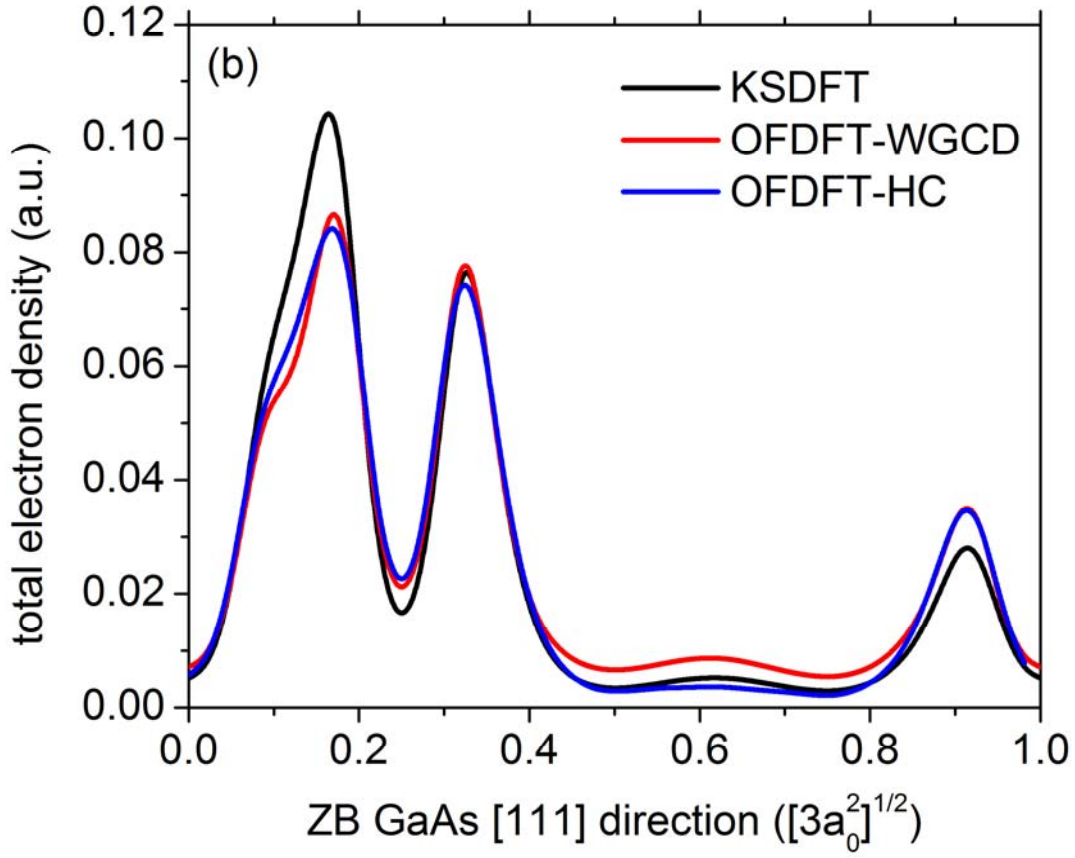

Figure 8. KSDFT, OFDFT-WGCD and OFDFT-HC self-consistent electron densities along the [111] direction in (a) CD Si and (b) ZB GaAs at their own equilibrium volumes. The horizontal axis is normalized by $(3a_0^2)^{1/2}$, where a_0 is the equilibrium lattice constant in the KSDFT and OFDFT calculations, respectively. For CD Si, the two Si atoms are at 0.0 and 0.25; for ZB GaAs, the Ga atom is at 0.0 and the As atom is at 0.25. In the OFDFT calculations employing the HC KEDF, λ=0.01 and β=0.65 are used for CD Si and λ=0.013 and β=0.783 for ZB GaAs.[49] In the OFDFT calculations employing the WGCD KEDF, a=0.864, b=0.67 and m=0 are used for CD Si and a=0.823, b=0.732 and m=0 for ZB GaAs.

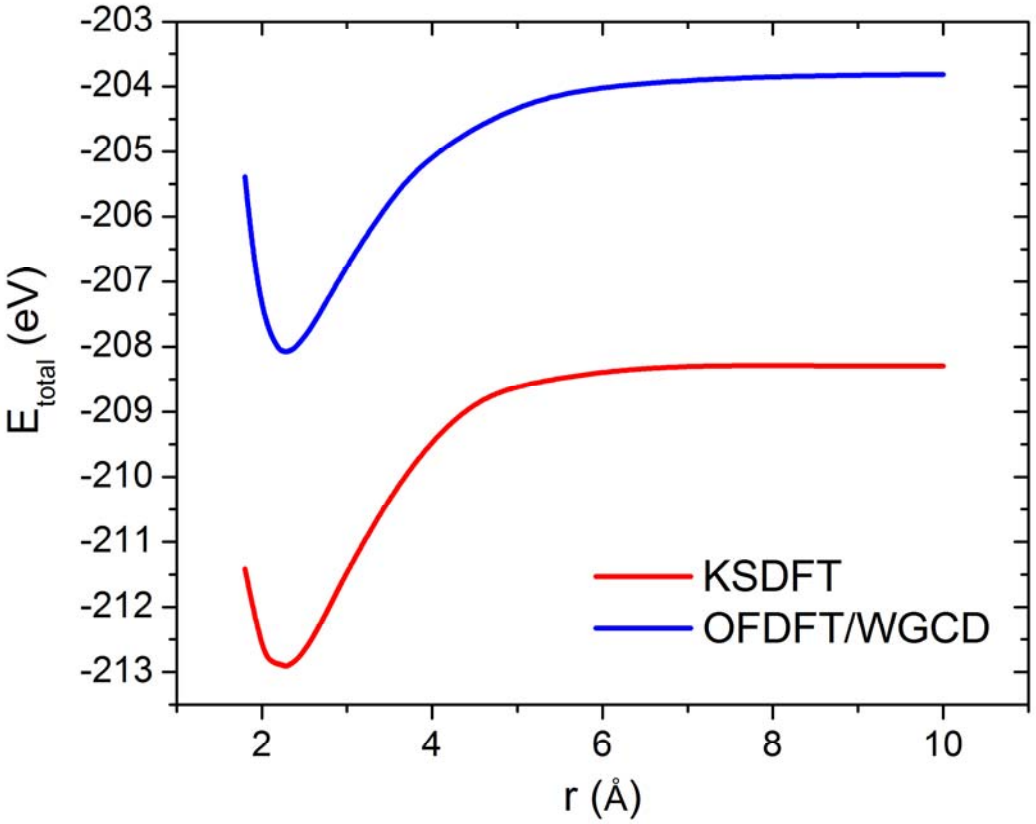

Figure 9. Total energy versus bond length curves for M_S = 0 Si_2 calculated by KSDFT and the OFDFT-WGCD model. a=0.864, b=0.670 and m=0 are used in the WGCD KEDF and ρ_c=5×10^{-5} a.u. is employed in calculating an average density here where vacuum is present.